Acta Pharmaceutica Sinica B 2025;15(11):6052−6069

Chinese Pharmaceutical Association
Institute of Materia Medica, Chinese Academy of Medical Sciences

Acta Pharmaceutica Sinica B

www.elsevier.com/locate/apsb
www.sciencedirect.com

ORIGINAL ARTICLE

Orally deliverable biomimetic nucleic acid therapies for targeted treatment of atherosclerosis

Chenwen Li[a,b,†], Yidan Chen[a,†], Yuan Li[c,†], Huan Liu[a,d,†], Shengqian Yang[a], Yongyao Lin[a], Yuantong Qi[a], Songling Han[e], Yin Dou[a], Gaoxing Luo[e,*], Yingxue Hao[d,*], Jianxiang Zhang[a,b,e,*]

[a]*Department of Pharmaceutics, College of Pharmacy, Third Military Medical University (Army Medical University), Chongqing 400038, China*
[b]*Yu-Yue Pathology Scientific Research Center, Chongqing 400039, China*
[c]*Department of Neurology, Southwest Hospital, Third Military Medical University (Army Medical University), Chongqing 400038, China*
[d]*Department of Vascular Surgery, Southwest Hospital, Third Military Medical University (Army Medical University), Chongqing 400038, China*
[e]*State Key Laboratory of Trauma and Chemical Poisoning, Third Military Medical University (Army Medical University), Chongqing 400038, China*

Received 8 October 2024; received in revised form 20 February 2025; accepted 16 April 2025

KEY WORDS

Atherosclerosis;
Nucleic acid;
Microcapsule;
Oral delivery;
Targeted therapy;
Lymphatic transport;
microRNA-33;
Cholesterol efflux

Abstract Accumulating evidence has demonstrated that nucleic acid-based therapies are promising for atherosclerosis. However, nearly all nucleic acid delivery systems developed for atherosclerosis necessitate injection, which results in rapid elimination and poor patient compliance. Consequently, oral delivery strategies capable of targeting atherosclerotic plaques are imperative for nucleic acid therapeutics. Herein we report the development of yeast-derived capsules (YCs) packaging an antisense oligonucleotide (AM33) targeting microRNA-33 (miR-33) for the oral treatment of atherosclerosis. YCs provide stability for AM33, preventing its premature release in the gastrointestinal tract. AM33-containing YCs, defined as YAM33, showed high transfection in macrophages, thus promoting cholesterol efflux and inhibiting foam cell formation by regulating the target genes/proteins of miR-33. Orally delivered YAM33 effectively accumulated within atherosclerotic plaques in *ApoE*$^{-/-}$ mice, primarily by transepithelial absorption

*Corresponding authors.
E-mail addresses: logxw@tmmu.edu.cn (Gaoxing Luo), haoyingxue@hotmail.com (Yingxue Hao), jxzhang1980@gmail.com, jxzhang@tmmu.edu.cn (Jianxiang Zhang).
[†]These authors made equal contributions to this work.
Peer review under the responsibility of Chinese Pharmaceutical Association and Institute of Materia Medica, Chinese Academy of Medical Sciences.

https://doi.org/10.1016/j.apsb.2025.07.039

via M cells in Peyer's patches and subsequent translocation *via* macrophages through the lymphatic system. Inhibition of miR-33 by oral YAM33 significantly delayed the progression of atherosclerosis. Moreover, oral treatment with YCs co-delivering AM33 and atorvastatin afforded significantly enhanced anti-atherosclerotic effects. Our findings suggest that yeast-based microcapsules represent an effective carrier for oral delivery of nucleic acids, either alone or in combination with existing drugs, offering a promising approach for precision therapy of atherosclerotic diseases.

1. Introduction

Despite considerable progress in the treatment of atherosclerotic cardiovascular diseases, the mortality rate resulting from myocardial infarction and stroke remains the leading cause of death worldwide[1]. Currently, statins and proprotein convertase subtilisin/kexin type (PCSK) 9 inhibitors capable of lowering the levels of low-density lipoprotein (LDL) are the most common drugs clinically used for the treatment of atherosclerosis[2-4]. However, these lipid-lowering therapies afford limited efficacy in the regression of atherosclerosis, and treatment with these drugs only showed a 20%−40% reduction in subsequent major coronary events[5,6]. Furthermore, long-term systemic administration of these drugs may cause various side effects, including diabetes, rhabdomyolysis, liver injury, and nasopharyngitis, mainly due to the non-specific distribution of drug molecules. Moreover, due to the high cost of PCSK9 inhibitors, their applications impose a heavy financial burden on patients[7,8]. Consequently, more specific, effective, and safe therapies capable of promoting atherosclerosis regression are imperative for the management of many cardiovascular diseases.

Increasing evidence has demonstrated that nucleic acid-based therapies hold great promise for the treatment of atherosclerosis. In addition to DNA therapies, different types of RNA therapeutics have been evaluated in preclinical and clinical studies for treating atherosclerotic diseases, including antisense oligonucleotides (ASOs), small interfering RNAs (siRNAs), microRNA (miRNA) mimetic and inhibitor therapies, and messenger RNA (mRNA)[9-14]. Of note, Volanesorsen, an ASO targeting hepatic apolipoprotein C-III mRNA was approved by the European Union in 2019, for the treatment of adult patients with familial chylomicronemia syndrome, hypertriglyceridemia, and familial partial lipodystrophy[15-17]. Most recently, inclisiran, a siRNA therapy capable of notably reducing PCSK9 synthesis in the liver and decreasing cholesterol levels, has been approved by the Food and Drug Administration of USA in 2021[9,12,18]. For therapeutic applications of RNA therapeutics, different chemical modification approaches have been developed to enhance their stability, target affinity, and tissue/cell uptake efficiency[13,14,19]. Alternatively, various classes of nonviral delivery vectors, such as liposomes, lipid nanoparticles, exosomes, polymeric micelles, dendrimers, lipoprotein-based carriers, DNA nanostructures, and bioresponsive nanoparticles are examined or used to achieve local or site-specific delivery of RNA therapies to target tissues or cells[10,19-27]. However, nearly all delivery systems for nucleic acid therapeutics developed thus far need to be administered *via* injection, particularly intravenous injection, to realize desirable targeting effects[23,27]. Meanwhile, their targeting capability mainly relies on direct penetration through the impaired endothelium or the disrupted vasculature[28-31], which can be considerably impaired by unexpected surface coating of biomolecules in the blood and rapid elimination *via* the mononuclear phagocytic system. Moreover, intravenous injection is invasive and often results in poor patient compliance. This is particularly concerning for chronic diseases like atherosclerosis, which typically require lifelong treatment. Therefore, there is a critical need to develop safe, effective, patient-friendly, and innovative delivery strategies to facilitate the clinical translation of existing nucleic acid therapies.

Oral delivery is the preferred route for treating chronic diseases that necessitate frequent administration, due to its numerous advantages, including non-invasiveness, convenience, cost-effectiveness, favorable safety performance, high patient acceptance and adherence, and ease of dosage adjustment[32-34]. However, oral delivery of a sufficient amount of nucleic acid molecules to atherosclerotic plaques is extremely challenging, due to the harsh gastrointestinal environment, low absorption/bioavailability, and long way before translocation to aortic lesions. Previously, we discovered that microcapsules derived from *Saccharomyces cerevisiae* yeast can be transported to distant inflammatory sites in murine models of tumors and arthritis after oral administration[35,36]. For these yeast-derived capsule (YC) delivery systems, their oral targeting to inflammation is mainly mediated by Dectin-1-based transcytosis *via* M cells in intestinal Peyer's patches and sequential endocytosis in monocytes/macrophages, which are then translocated to neighboring lymphoid tissues and finally delivered to remote inflammatory sites[35,37-39]. Of note, YCs can efficiently load different types of therapies, varying from small-molecule drugs, and peptides/proteins, to nucleic acids[35,37-43].

Based on these encouraging findings, herein we hypothesize that YCs can serve as an efficient platform for site-specifically delivering nucleic acid therapeutics to aortic plaques *via* the oral route (Fig. 1), thereby realizing targeted treatment of atherosclerosis. As a proof of concept and with the aim to develop an effective and safe oral deliverable nucleic acid therapy, anti-miR33 (AM33), an ASO targeting intronic microRNA-33-5p (miR33) was used as a candidate drug, since accumulative evidence indicates that miR-33 plays a pivotal role in the pathogenesis of atherosclerosis[44,45]. miR33 is located within the gene encoding sterol-regulatory element-binding factor-2 (SREBF-2), a well-recognized transcriptional regulator of genes involved in cholesterol biosynthesis and cellular cholesterol transport. miR33 can suppress the expression of adenosine triphosphate-binding cassette transporters A1 (*ABCA1*) and G1 (*ABCG1*) genes[46], thus attenuating the cholesterol efflux and decreasing biosynthesis of high-density lipoprotein (HDL)[44,47,48]. By contrast, miR-33 antagonism with AM33 affords atheroprotective effects by regulating cholesterol and fatty acid synthesis/uptake, raising plasma HDL, lowering very low-density

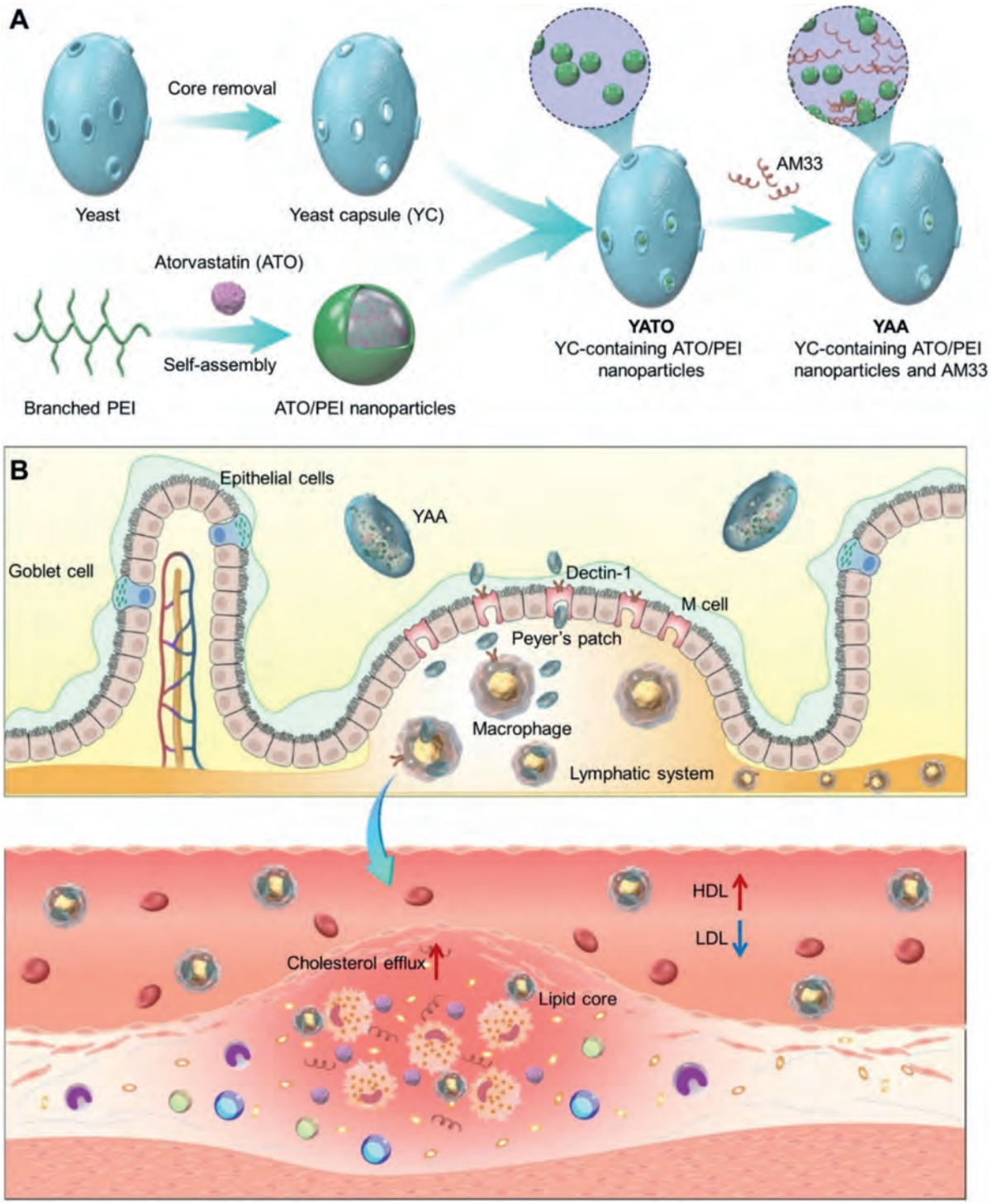

Figure 1 Schematic illustration of the composition and engineering of orally deliverable nucleic acid therapies based on yeast-derived biomimetic microcapsule (YCs) containing atorvastatin (ATO) and anti-miR33 (AM33) for targeted treatment of atherosclerosis. (A) A sketch showing the engineering of orally deliverable YC therapies containing ATO and AM33. (B) Translocation and targeted atherosclerotic treatment *via* orally delivered YCs loaded with ATO and AM33.

lipoprotein levels, and reprograming the immune cell landscape in plaques[49,50]. Besides demonstrating the targeting and therapeutic effects of orally delivered AM33-loaded YCs, we attempt to substantiate that YCs can site-specifically co-deliver nucleic acid and small-molecule therapeutics to achieve synergistic anti-atherosclerotic efficacies.

2. Materials and methods

2.1. Materials

Yeast of *Saccharomyces cerevisiae* was obtained from Lesaffre International Corporation (France). The oligonucleotide

anti-miR33 (TGCAATGCAACTACAATGCAC, defined as AM33) and Cy3-labeled anti-miR33 (Cy3-AM33) were biosynthesized by Ribo Life Science Co., Ltd. (Suzhou, China). Atorvastatin (ATO) was purchased from Aladdin Biochemical Technology Co., Ltd. (Shanghai, China). Branched polyethyleneimine (PEI) with molecular weight (Mw) of 25 kDa, fluorescein isothiocyanate (FITC), DNase I, collagenase I, collagenase XI, and hyaluronidase were purchased from Sigma−Aldrich (USA). Anti-ABCA1 antibody, anti-ABCG1 antibody, and anti-CD68 antibody were supplied by Abcam (USA). 25-[*N*-[(7-Nitro-2-1,3-benzoxadiazol-4-yl) methyl] amino]-27-norcholesterol (NBD-cholesterol), cell counting kit-8 (CCK-8) and all ELISA kits were obtained from Boster (Wuhan, China). Lipopolysaccharide (LPS) and 4′,6-diamidino-2-phenylindole (DAPI) were purchased from Beyotime (Shanghai, China). LysoTracker Green was obtained from Invitrogen (USA). Human oxidized low-density lipoprotein (ox-LDL) and purified human high-density lipoprotein (HDL) were purchased from Yiyuan Biotechnologies (Guangzhou, China). Cycloheximide (CXI) was obtained from MedChemExpress LLC (USA). All the other reagents are commercially available and used as received.

2.2. Preparation of yeast microcapsules

Yeast microcapsules (YCs) were prepared following the procedures described in our previous study[38]. Briefly, 50 g yeast was suspended in 500 mL of 1 mol/L NaOH, and the resulting slurry was heated at 80 °C for 1 h. The sample was retrieved by centrifugation at 2200×*g* (Eppendorf) for 15 min, rinsed twice with deionized water, dispersed in aqueous solution at pH 4.5, and then incubated at 55 °C for 1 h. After centrifugation and comprehensive washing with deionized water, the yeast sample was rinsed four times with isopropyl alcohol and additionally washed with acetone twice. Finally, the yeast sample was collected and dried under vacuum.

2.3. Synthesis of FITC-conjugated PEI

To synthesize FITC-conjugated PEI (FITC-PEI), 4 mg FITC in 2 mL of DMSO was added into 4.5 mL of DMSO containing 36 mg PEI. The obtained solution was stirred in the dark at 37 °C for 4 h. After complete reaction, FITC-PEI was obtained by dialysis of the reaction solution against deionized water for 24 h.

2.4. Preparation of PEI-containing YCs

To prepare PEI-loaded YC (YC-PEI), a certain amount of YC was dispersed in deionized water by sonication, and different contents of PEI in aqueous solution was added with the weight ratio of PEI to YC ranging from 0.02:1 to 0.5:1. The mixture was incubated at 37 °C for 4 h. YC-PEI was obtained after centrifugation and rinsing with deionized water. FITC-labeled YC-PEI was fabricated through similar procedures by packaging FITC-PEI in YCs.

2.5. Self-assembly of ATO/PEI nanoparticles

ATO-loaded PEI nanoparticles (ATO-PEI NP) were prepared by self-assembly. In brief, different contents of ATO and 10 mg PEI were co-dissolved in 1 mL of DMSO (the weight ratio of ATO to PEI ranging from 1:1, 1.25:1, 1.75:1, 2.5:1, to 5:1), and then dialyzed against deionized water for 24 h at room temperature. The aqueous solutions containing ATO/PEI nanoparticles were collected for further experiments.

2.6. Preparation of YCs packaged with AM33 or ATO

To package AM33 into YC, 3.8 mg YC-PEI (at a PEI/YC weight ratio of 0.1:1) was suspended in 10 mL of deionized water and stirred at 37 °C for 30 min. An appropriate amount of AM33 (5 nmol) was added, followed by stirring at 37 °C for 2 h. AM33-loaded YC (YAM33) was obtained by centrifugation at 2000×*g* for 10 min, washing with deionized water, and freeze-drying. Similarly, Cy3-AM33-loaded YC (*i.e.*, Cy3-YAM33) was prepared.

To load ATO into YC, 15 mg YC was suspended in 10 mL of deionized water. 1.5 mg of ATO/PEI nanoparticles (obtained at an ATO/PEI weight ratio of 1:0.6) was added and incubated at 37 °C for 4 h. After centrifugation at 2000×*g* for 5 min, rinsing with deionized water 3 times, and freeze-drying, ATO-loaded YC (defined as YATO) was obtained.

To prepare YC co-loaded with AM33 and ATO, 70 mg YATO was suspended in 100 mL of deionized water, into which 7 mg PEI was added and stirred at 37 °C for 2 h. The obtained solution was centrifuged and washed with deionized water to remove un-loaded PEI, and then 100 nmol AM33 was added. After 4 h of incubation at 37 °C, YC containing both ATO and AM33 (defined as YAA) was collected by centrifugation, rinsing with deionized water, and lyophilization.

2.7. Characterization of various particles

Particle size and ζ-potential measurements were performed on a Malvern Zetasizer Nano ZS instrument (Britain) at 25 °C. Scanning electron microscopy (SEM) was carried out on a FIB-SEM microscope (Crossbeam 340, Zeiss, Germany), while transmission electron microscopy (TEM) observation was conducted on a Tecnai-10 microscope (Philips, the Netherlands) operating at an acceleration voltage of 80 kV. Confocal laser scanning microscopy (CLSM) observation was performed by a Zeiss LSM510 laser scanning confocal microscope (Germany).

To quantify the content of ATO in ATO/PEI nanoparticles, the lyophilized sample of ATO/PEI nanoparticles was dispersed in methanol to extract ATO. Then high-performance liquid chromatography (HPLC, LC-20A, Shimadzu, Japan) was performed to determine the concentration of ATO. The detection wavelength was 244 nm, while the mobile phase consisted of deionized water and methanol (*v*/*v*, 65:35), with a flow rate of 1.0 mL/min. The content of ATO in YATO and YAA was detected through similar procedures. On the other hand, AM33 entrapped in YAM33 or YAA was determined by quantifying un-loaded AM33 in an aqueous solution *via* fluorescence measurement of Cy3-AM33. The excitation and emission wavelengths were set at 550 and 570 nm, respectively.

2.8. In vitro stability and release studies

The stability of YAM33 was tested at 37 °C in deionized water, 0.01 M PBS (pH 7.4), or saline. At different time points, the content of Cy3-AM33 in the supernatant was measured by fluorescence spectroscopy (F-7000, Hitachi, Japan). For *in vitro* release tests, 10 mg Cy3-YAM33 or YAA was dispersed in 4.0 mL of aqueous solution and placed into dialysis tubing, which was then immersed in 40 mL of simulated gastric fluid at pH 1.2 and incubated at 37 °C. After 2 h, the dissolution medium was changed to simulated intestinal fluid at pH 7.4. At specific time intervals, 3 mL of release medium was withdrawn, and fresh medium was supplemented. The AM33 concentrations in release

buffers were quantified by fluorescence spectroscopy, while the amount of ATO was detected by HPLC. Meanwhile, the morphology of YAM33 was observed by TEM and CLSM at different time points.

Also, the stability of AM33 in gastrointestinal fluid was evaluated by agarose gel electrophoresis. Briefly, 200 μL of aqueous solution containing YAM33 or free AM33 (at 0.5 mg/mL of AM33) was incubated at 37 °C for 4 h in 0.2 mL of simulated gastric fluid or simulated intestinal fluid. Then the solution was loaded on a 1.2% agarose gel for 30 min at 120 V. YAM33 and free AM33 without any treatment were employed as controls. The gel images were acquired using a Chemiluminescence Imaging System (Vilber Bio Imaging, France).

In a separate study, 100 μL of aqueous solution containing YATO or free ATO (at 0.5 mg/mL of ATO) was incubated at 37 °C for 4 h in 0.2 mL of simulated gastric fluid or simulated intestinal fluid. Then the solution containing free ATO was filtrated through a 0.22-μm microporous filter membrane and detected by HPLC. Meanwhile, the solution from the YATO group was centrifuged and 300 μL of methanol was added to the precipitate. The mixture was sonicated for 10 min to allow complete extraction of ATO from YCs. Following centrifugation, the ATO content in the supernatant was determined by HPLC.

2.9. Animals

All animal care and experimental protocols were conducted in accordance with the rules of the Animal Ethical and Experimental Committee of the Third Military Medical University (Army Medical University, Chongqing, China; approval number AMUWEC2019122). Male apolipoprotein E-deficient ($ApoE^{-/-}$) mice (about 6 weeks old) were supplied by the Vital River Co., Ltd. (China). Male C57BL/6 mice (6−8 weeks) were obtained from the Animal Center of the Army Medical University. All mice were acclimatized for at least 7 days before further experiments.

2.10. Cell culture

RAW264.7 mouse macrophages were purchased from the Institute of Biochemistry and Cell Biology (Shanghai, China). The cells were cultured in RPMI 1640 medium supplemented with 10% fetal bovine serum (FBS) and penicillin/streptomycin at 37 °C in a humidified atmosphere containing 5% CO_2.

Also, bone marrow-derived macrophages (BMDMs) were differentiated from mouse bone marrow cells. In brief, C57BL/6 mice of 4 weeks' old were sacrificed and the leg bones were isolated. After the epiphyses of the bones were cut, the marrow was flushed with Dulbecco's modified Eagle's medium (DMEM) using a 5-mL syringe. The cell suspension was centrifuged at 250×*g* for 10 min. The cell pellet was treated with red blood cell lysate, then resuspended in DMEM and passed through 70-μm cell strainers. BMDMs were acquired by *in vitro* differentiation of the collected cells in the presence of macrophage colony-stimulating factor for 7 days.

2.11. In vitro cellular uptake

RAW264.7 cells were seeded on a glass cover slide in 12-well plates at a density of 1×10^5 cells/well. After 12 h, the culture medium was replaced with fresh medium containing Cy3-YAM33 (at 0.2 nmol/L of Cy3-AM33) and incubated for various durations. Before observation, nuclei were stained with DAPI, while endosomes/lysosomes were stained with LysoTracker Green for 1 h. Fluorescence images were acquired by CLSM. Dose-dependent internalization was performed after incubation for 3 h in the same manner. Additionally, cellular internalization of free Cy3-AM33 in RAW264.7 cells was examined after 3 h of incubation.

To quantify the extent of YAM33 internalization, RAW264.7 cells were seeded in 12-well plates and incubated overnight. After the cells were incubated with Cy3-YAM33 at defined doses for specified time periods, the cells were harvested and fluorescence intensities were quantified *via* flow cytometry (BD FACSCelesta, USA). Through similar procedures, time- and dose-dependent cellular uptake of Cy3-YAM33 in BMDMs was also investigated.

2.12. In vitro cholesterol efflux assay

The effect of YAM33 treatment on cholesterol internalization was first explored. To this end, RAW264.7 macrophages in 24-well plates (5×10^4 cells per well) were pretreated with a medium containing free AM33 or various concentrations of YAM33 for 8 h. Then, the medium was removed and changed to NBD-cholesterol at 1 μg/mL, followed by 4 h of incubation. The cells were washed and lysed in 0.1% Triton X-100 and the fluorescence intensities of NBD-cholesterol in the cell lysates were measured by fluorescence spectroscopy. The excitation and the emission wavelengths were set at 465 nm and 535 nm, respectively.

In vitro cholesterol efflux was performed based on a previously reported method with slight modification[25]. Briefly, RAW264.7 macrophages in 24-well plates at a density of 5×10^4 cells per well were incubated with phenol red-free RPMI 1640 medium containing 1 μg/mL NBD-cholesterol for 4 h. After cholesterol loading, the cells were treated with free AM33 or various concentrations of YAM33 in the presence of 10 μg/mL HDL for 8 h. Then the cells were lysed in 0.1% Triton-X100 and the fluorescence intensities of NBD-cholesterol in the cell lysates were measured. Following similar procedures, the effects of different concentrations of blank YCs on cholesterol efflux were also examined.

2.13. Studies on foam cell formation in vitro

RAW264.7 macrophages were stimulated with 0.1 μg/mL LPS for 12 h. The medium was then replaced with fresh medium containing free AM33 (0.2 nmol/L) or gradient concentrations of YAM33 and incubated for 4 h. The cells were treated with 50 μg/mL ox-LDL for 48 h. Subsequently, cells were rinsed twice with PBS and fixed in 4% paraformaldehyde, then stained with 0.3% Oil Red O (ORO) for 30 min. The formation of foam cells was assessed by optical microscopy. Similarly, the effect of blank YCs on foam cell formation was also investigated.

To examine the bioactivity of YAM33 after crossing the epithelial barrier, Caco-2 cells were cultured (1×10^5 cells/well) on the polycarbonate membranes of Transwell plates (Corning Costar Corp). Then the apical solution was replaced with fresh medium containing YAM33 at 1 nmol/L AM33. After 8 h, the medium at the basolateral side was collected to evaluate its effects on the foam cell formation in ox-LDL-induced macrophages.

2.14. Quantitative real-time PCR (qRT-PCR)

RAW264.7 macrophages in 12-well plates at a density of 3×10^5 cells per well were incubated with free AM33 or various

concentrations of YAM33 for 2 h. Total RNA was extracted from transfected cells using the TRNzol Universal Reagent (Tiangen Biotech Co., Ltd., Beijing, China). cDNA was amplified using an iScript cDNA Synthesis Kit (Bio-Rad, USA), and gene expression was measured by qRT-PCR using SYBR Green PCR Supermix (Bio-Rad, USA). β-Actin served as a control. Gene-specific primers are summarized in Supporting Information Table S1.

2.15. Analysis of ABCA1 and ABCG1 expressions

RAW264.7 macrophages in 12-well plates (3×10^5 cells per well) were treated with medium containing free AM33 or various concentrations of YAM33 for 4 h. Subsequently, macrophages were labeled with ABCA1 antibodies and Alexa Flour 488-labeled secondary antibody. After washing twice with PBS, samples were analyzed by flow cytometry.

In a separate study, RAW264.7 cells were seeded on a glass cover slide in 12-well plates at a density of 3×10^5 cells/well. After 12 h, the culture medium was replaced with fresh medium containing free AM33 or various concentrations of YAM33 and incubated for 4 h. Before observation, cells were stained with ABCG1 antibody and Alexa Fluor 488-labeled secondary antibody. Fluorescence images were acquired by CLSM after counterstaining with DAPI.

2.16. In vitro anti-inflammatory effects

RAW264.7 macrophages were seeded in 12-well plates, into which LPS at 0.5 μg/mL was added. After incubation for 3 h, free AM33 or different doses of YAM33 were added and incubated for another 6 h. The levels of tumor necrosis factor (TNF)-α, interleukin (IL)-1β, and IL-6 in the supernatant were determined by ELISA.

2.17. In vitro cytotoxicity

RAW264.7 macrophages or BMDMs were seeded in 96-well plates at a density of 1×10^4 cells per well and incubated overnight. Then different doses of YAM33 or YAA (varying from 0.05, 0.1, 0.2, 0.5, 1.0, to 2.0 nmol/L) were added. After incubation for 24 h, cell viability was determined by Cell Counting Kit (CCK)-8.

2.18. In vivo atherosclerotic plaque targeting effects of YAM33 in $ApoE^{-/-}$ mice

Atherosclerotic plaques in male $ApoE^{-/-}$ mice were induced by feeding a high-fat diet containing 20% lard and 1.25% cholesterol for 3 months. Then Cy3-YAM33 at 20 mg/kg was orally administered to C57BL/6 mice or $ApoE^{-/-}$ mice, while C57BL/6 mice in the control group were treated with the same dose of YAM33. Animals were sacrificed at 12 h after oral gavage. The aortas were resected and imaged on an IVIS spectrum system (PerkinElmer, USA).

In a separate study, $ApoE^{-/-}$ mice with advanced atherosclerosis were separately administered with Cy3-YAM33 or Cy3-labeled AM33/PEI complexes (*i.e.*, Cy3-PAM33) at 20 mg/kg of Cy3-AM33 by oral gavage. At 12 h after administration, mice were euthanized and different organs/tissues, including the aorta, Peyer's patch (PP), mesenteric lymph node (MLN), inguinal lymph node (ILN), liver, spleen, lung, kidney, and intestine, were isolated for *ex vivo* imaging.

2.19. Studies on the transportation processes and mechanisms of YAM33 after oral delivery

Cy3-YAM33 at 20 mg/kg was orally gavaged in $ApoE^{-/-}$ mice fed a high-fat diet for 3 months. At 3 and 12 h post-administration, mice were euthanized. Then the aorta, PP, MLN, ILN, and main organs were isolated and imaged by the IVIS spectrum system. Additionally, the fragments of aortic tissues and PP were suspended in a mixture of DNase I (60 U/mL), hyaluronidase (60 U/mL), collagenase I (450 U/mL), and collagenase XI (125 U/mL) at 37 °C for 40 min. The obtained suspension was passed through a 70-μm cell strainer, centrifuged, and cultured in DMEM for 4 h. Then the cells were rinsed and the attached cells were fixed in 4% paraformaldehyde, stained with rat anti-mouse CD68 antibody, and FITC-labeled goat anti-rat IgG (H + L), while nuclei were stained with DAPI. Images were acquired using a Zeiss confocal microscope.

To further investigate the transport mechanism of YAM33, laminarin was used to assess its inhibitory effect on intestinal adsorption of YAM33. In this case, C57BL/6 mice were randomly divided into 3 groups. The control group received oral saline administration, while the other two groups were treated with Cy3-YAM33 at 20 mg/kg of Cy3-AM33 by oral gavage with or without pre-treatment with laminarin at 15 mg/kg for 1 h prior to Cy3-YAM33 ingestion. Animals were sacrificed 4 h after administration, and the PP tissue was harvested and imaged by an IVIS spectrum system. Subsequently, the PP was embedded in Tissue-Tek O.C.T. Compound and 7 μm-thick cryosections were prepared and stained with anti-GP2 antibody (MBL International Corporation, Japan) at 2.5 μg/mL in the dark at 4 °C for 12 h. Then the sections were incubated with corresponding FITC-labeled secondary antibody (1:250; Beyotime, Shanghai, China) at 37 °C for 30 min. Nuclei were counterstained with DAPI. Images were captured by a Zeiss confocal microscope.

Moreover, CXI was employed to further examine the effect of lymphatic transport on intestinal absorption and plaque-targeting capacity of orally delivered YAM33. Briefly, $ApoE^{-/-}$ mice fed with a high-fat diet for 3 months were randomly divided into 5 groups. The control group received oral saline administration, while the other four groups were orally administrated with Cy3-YC, Cy3-AM33, Cy3-YAM33, or Cy3-YAM33 plus oral pre-treatment with CXI at 3 mg/kg 1 h prior to Cy3-YAM33 delivery. Animals were sacrificed at 12 h after administration, and the aorta, PP, MLN, ILN, and intestinal tissues were isolated for *ex vivo* imaging.

Subsequently, the integrity of YAM33 before and after crossing the intestinal epithelial barrier was examined. To this end, saline or Cy3-YAM33 (at 20 mg/kg of Cy3-AM33) was orally administrated to C57BL/6 mice. At 4 h post-administration, mice were euthanized, and the small intestine and PP tissues were isolated, embedded in Tissue-Tek O.C.T. Compound, frozen sliced, and stained with DAPI. Fluorescence images were acquired by CLSM.

2.20. In vivo anti-atherosclerotic efficacy of various formulations

$ApoE^{-/-}$ mice were fed with a high-fat diet for 3 months. After the first month, all mice were randomly assigned to five groups, which received various treatments every three days for an additional 2 months. Mice in the model group were orally treated with saline. The AM33 group was treated by subcutaneous injection of free AM33 at 5 mg/kg. The PAM33 group was orally administered with PAM33 at 5 mg/kg of AM33, while two YAM33 groups were

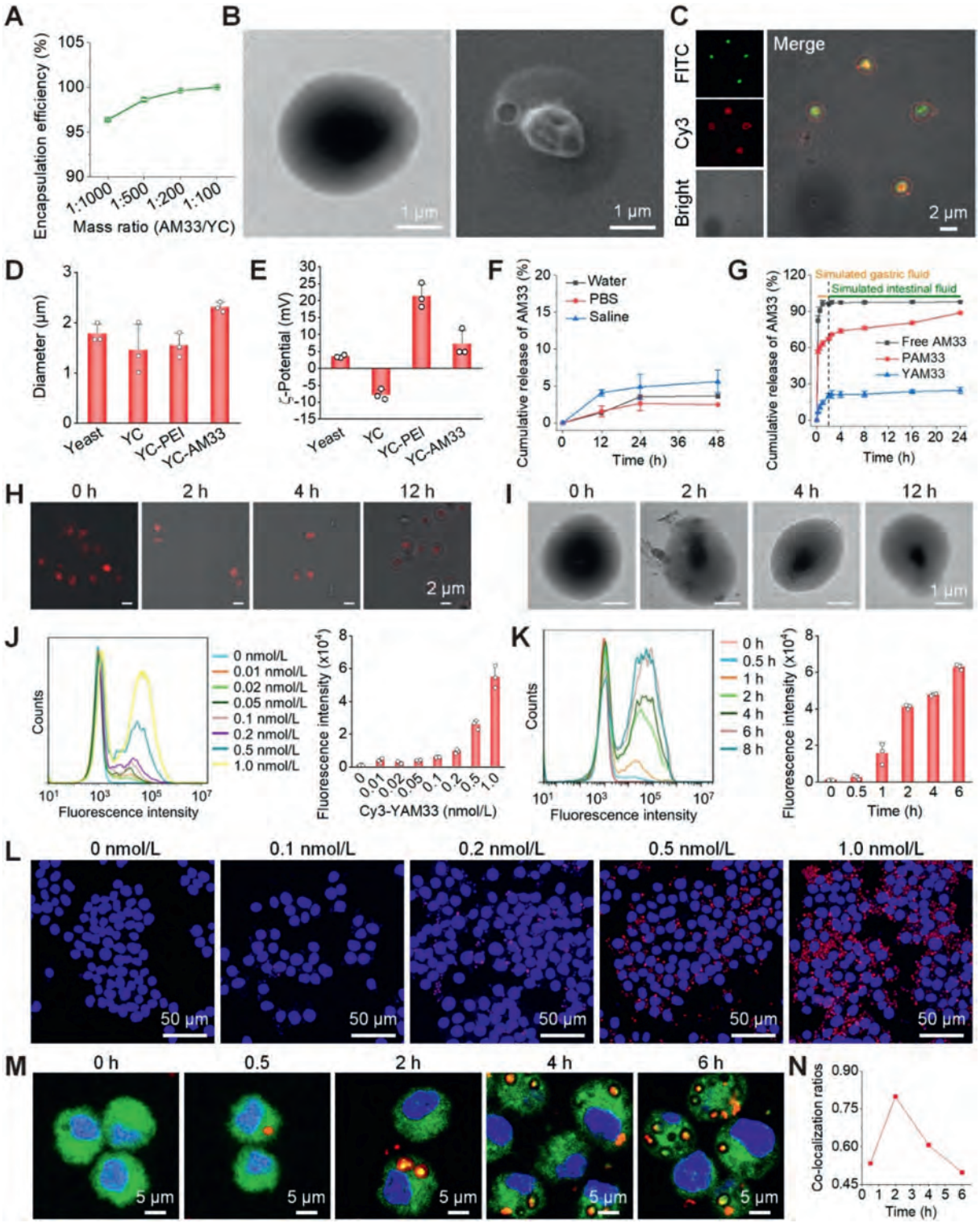

Figure 2 Rational design, screening, and characterization of AM33-loaded YCs (YAM33). (A) The loading efficiency of AM33 in PEI-deposited YC at different weight ratios of AM33 to YC. (B) TEM (left) and SEM (right) images of the finally screened YAM33. (C) Typical fluorescence images of YAM33. PEI was labeled with FITC (green), while AM33 was labeled with Cy3 (red). (D, E) Size (D) and ζ-potential (E) values of various formulations. (F) *In vitro* release of AM33 from YAM33 in various media. (G) *In vitro* release profiles of AM33 from different formulations in solutions simulating gastrointestinal conditions. (H, I) Confocal microscopy (H) and TEM (I) images of YAM33 at various time points after incubation in simulated gastrointestinal fluid. (J) Representative flow cytometric profiles (left) and quantification (right) show dose-dependent internalization of Cy3-YAM33 in macrophages after 3 h of incubation. (K) Flow cytometric curves (left) and quantification (right) of time-dependent uptake of Cy3-YAM33 in macrophages. (L) Fluorescence images indicating dose-dependent cellular uptake of Cy3-YAM33 in macrophages. (M, N) Fluorescence images (M) and quantified co-localization ratios (N) show intracellular trafficking of

treated with a low dose of YAM33 (at 5 mg/kg of AM33) and a high dose of YAM33 (at 20 mg/kg of AM33) by oral gavage. After different treatments, mice were euthanized. The whole aorta, blood, and main organs including the stomach, intestine, liver, spleen, lung, and kidney were collected to evaluate therapeutic effects and possible adverse effects. The possible *in vivo* efficacy of blank YCs was also examined following similar procedures.

In another cohort study, $ApoE^{-/-}$ mice were fed with a high-fat diet for 4 months to induce advanced atherosclerotic plaques. After the first month, all mice were randomly assigned to five experimental groups, which were orally administered with saline, free ATO at 7.8 mg/kg, YATO at 7.8 mg/kg of ATO, YAM33 at 5 mg/kg of AM33, or YAA at 5 mg/kg AM33 and 7.8 mg/kg ATO every three days for additional 3 months. Then similar procedures as mentioned above were followed.

2.21. Measurement of atherosclerotic plaques

To assess the degree of atherosclerotic lesions, the aortas were fixed in 4% paraformaldehyde for 24 h. Then they were opened longitudinally and stained with ORO. Additionally, the aortic root and liver were embedded in the Tissue-Tek O.C.T. Compound. Serial sections were prepared and stained with ORO. The plaque areas were quantified by Image-Pro Plus 6.0 software (Media Cybernetics, USA).

2.22. Histology and immunohistochemistry

The sections of the aortic root were separately stained with ORO, Masson's trichrome, anti-CD68 antibody, anti-TNF-α antibody, or anti-IL-1β antibody. The sections of major organs were stained with hematoxylin and eosin (H&E). Then optical microscopy images were acquired and quantitative analysis was performed.

2.23. Quantitative analyses of blood samples

The collected blood samples were analyzed for quantification of biochemical markers relevant to liver/kidney functions, hematological parameters, and plasma lipoprotein parameters including total cholesterol, triglyceride, and HDL.

2.24. Western blot analysis

Proteins were extracted from RAW264.7 cells or aorta tissues using the RIPA lysis buffer containing protease inhibitors based on the manufacturer's protocol. Then 15 μg protein samples were separated by SDS-PAGE gels, followed by transferring onto polyvinylidene difluoride membranes. Membranes were incubated with primary antibodies to ABCG1, ABCA1, or β-actin at 4 °C overnight, followed by incubation with appropriate secondary antibodies for 1 h. Detection was performed using a ChemiDoc Touch Imaging System (Bio-Rad, USA). The densitometry of each band was quantified by Image J.

2.25. Statistical analysis

All data are expressed as means ± standard deviation (SD). Statistical analyses were assessed by the one-way ANOVA test for data with more than two groups, and an unpaired *t*-test was conducted for experiments with two groups. Statistical significance was set at $P < 0.05$.

3. Results and discussion

3.1. Preparation and characterization of AM33-loaded YCs

YCs were fabricated by sequential treatment with alkali, acid, and organic solvents to remove the core contents[35,51], yielding microcapsules with an average diameter of 1.4 μm and ζ-potential of −7.7 mV. Compared to untreated yeasts, a substantial loss of cytoplasmic components in the obtained YCs was observed by TEM and SEM (Supporting Information Fig. S1). To enhance the loading capacity and transfection efficiency of AM33, a cationic polymer PEI was first introduced into the YC core. Initially, the effects of the weight ratio of PEI to YCs on the loading efficiency, ζ-potential, and cytotoxicity of resulting PEI-containing YCs (defined as YC-PEI) were interrogated. Blank YCs exhibited negative ζ-potential in deionized water, while the incorporation of PEI led to positive ζ-potential for the obtained YC-PEI. The loading efficiency of PEI and ζ-potential of YC-PEI notably increased with an increase in the PEI content. Nevertheless, the cell viability of YC-PEI-treated RAW264.7 macrophages decreased when the PEI feeding was enhanced (Supporting Information Fig. S2). After incubation at the same dose for 24 h, YC-PEI with the PEI/YC weight ratios at either 0.2:1 or 0.5:1 showed remarkably higher cytotoxicity as compared to blank YC. Consequently, the formulation with the PEI/YC weight ratio of 0.1:1 was used to prepare YC-PEI for the following experiments. Characterization by TEM and SEM revealed a similar shape and particle size for thus engineered YC-PEI, compared to blank YC, with an average diameter of 1.5 μm (Supporting Information Fig. S3A and S3B). CLSM observation showed intense green fluorescent signals of FITC-labeled PEI in YCs, indicating the successful entrapment of PEI (Fig. S3C).

Subsequently, the nucleic acid AM33 was packaged into YC-PEI through electrostatic interactions between cationic PEI and negative AM33, yielding AM-containing YC-PEI, which is termed YAM33. To optimize the entrapment efficiency of AM33 in YC, the effect of the AM33/YC weight ratio on AM33 loading was examined. The entrapment efficiency considerably increased with an escalating dose of AM33, and it was approximately 100% for the formulation with a weight ratio of AM33/YC at 1:100, which was selected to prepare YAM33 in the following experiments (Fig. 2A). After loading AM33, TEM and SEM observation showed a densely filled core in YC (Fig. 2B). CLSM images indicated considerable overlap of fluorescent signals from FITC and Cy3, which was used to label PEI and AM33, respectively, suggesting co-loading and complexation of PEI and AM33 (Fig. 2C). The average size of YAM33 was 2.3 μm, and its ζ-potential was 7.2 mV (Fig. 2D and E).

Upon incubation in water, 0.01 M PBS (pH 7.4), or saline for 48 h, YAM33 showed notably slow release profiles, demonstrating its good stability, which was largely due to the protection of YC walls (Fig. 2F). To assess the stability of AM33 within YAM33 in the harsh environment of the gastrointestinal tract, YAM33 was incubated with simulated gastric or intestinal fluids for 4 h at

Cy3-YAM33 in macrophages after incubation for various periods of time. Before observation, nuclei were stained with DAPI (blue), while endosomes/lysosomes were stained with LysoTracker (green). Data in (A, D−G, J−K) are mean ± SD ($n = 3$).

37 °C. The agarose gel electrophoresis results showed that AM33 encapsulated in YAM33 remained undetectable, while free AM33 was partially degraded, indicating the effective protection of AM33 by YCs (Supporting Information Fig. S4). *In vitro* release tests were then performed in media simulating the gastrointestinal pH conditions. We found evidently rapid dissolution of AM33 from free AM33 and PEI/AM33 nanoparticles (defined as PAM33) within 2 h in simulated gastric fluid, showing a cumulative release percentage >50%. After the release medium was switched to PBS simulating intestinal pH, nearly complete AM33 release was detected for PAM33 at 24 h. By contrast, notably slow release was observed for YAM33 at pH 1.2, and almost no release occurred in the simulated intestinal fluid (Fig. 2G). In line with these results, CLSM and TEM observation showed that the content of YAM33 was only reduced in the first 2 h and no obvious changes were observed in the next 10 h (Fig. 2H−I). Also, the shell of YCs was intact in this period. These results substantiated that the newly engineered YAM33 is able to protect the loaded nucleic acid from degradation and prevent its early release in the gastrointestinal environment.

3.2. *In vitro cellular evaluations of YAM33*

After oral administration, YCs will be predominantly transported to inflammatory sites through monocytes/macrophages, which recognize β-1,3-glucan on YCs *via* the membrane phagocytic pattern-recognition receptor Dectin-1[35,39]. Accordingly, we examined the cellular internalization of YAM33 in RAW264.7 macrophages and BMDMs, using Cy3-labeled AM33 (*i.e.*, Cy3-YAM33). Both flow cytometry quantification and CLSM observation revealed efficient endocytosis of Cy3-YAM33 in two types of macrophages, in time- and dose-dependent patterns (Fig. 2J−L and Supporting Information Figs. S5 and S6). Of note, RAW264.7 macrophages incubated with Cy3-YAM33 exhibited notably higher intracellular fluorescence intensities compared to those treated with free Cy3-AM33 at an equivalent dose of Cy3-AM33 (Supporting Information Fig. S7). In addition, staining of endolysosomes by LysoTracker (green fluorescence) suggested that endocytosed Cy3-YAM33 was transported in macrophages *via* the endolysosomal pathway (Fig. 2M and N). Moreover, although Cy3 fluorescence (red) was primarily co-localized with green fluorescence at 2 h after incubation, considerable Cy3 fluorescence alone was detected at 4 and 6 h, indicating effective endolysosomal escape at these time points, largely benefiting from the proton sponge effect-mediated rupture of endolysosomes induced by PEI[52,53]. By contrast, the extremely low level of Cy3-AM33 internalized in macrophages exhibited minimal lysosomal escape at all examined time intervals (Supporting Information Fig. S8). This suggests that encapsulation by YC can effectively promote cellular uptake and endolysosomal escape of AM33. Furthermore, we examined the retention and release profiles of YAM33 in macrophages. To this end, fluorescence changes in macrophages with endocytosed Cy3-YAM33 were detected. It was found that fluorescence intensities of Cy3-YAM33 in macrophages gradually decreased after incubation for different time periods (Supporting Information Fig. S9). Nevertheless, notable fluorescence of Cy3-YAM33 was still observed even at 24 h. This result implied that Cy3-YAM33 internalized in macrophages can be slowly released. The long-term retention of endocytosed YAM33 in macrophages is important to reduce therapeutic loss during translocation.

Previous studies have demonstrated that miR-33 can suppress cholesterol efflux by down-regulating the expression of ABCA1 and ABCG1, while inhibition of miR-33 effectively reverses its detrimental impact on cholesterol efflux[44,45]. Initially, we confirmed that YAM33 at various doses of AM33 had no significant effects on the cholesterol internalization in macrophages, in comparison to the control and free AM33 (Supporting Information Fig. S10). Then HDL-mediated cholesterol efflux in macrophages was examined. Compared to the fresh medium-treated control group, YAM33 treatment significantly enhanced cholesterol efflux in a dose-dependent pattern (Fig. 3A). Notably, blank YCs displayed minor effects on cholesterol efflux, while YAM33 showed remarkably higher activity in terms of improving cholesterol efflux than the equivalent dose of free AM33 and blank YCs (Supporting Information Fig. S11).

Subsequently, we interrogated whether treatment with YAM33 is effective in suppressing foam cell formation by inhibiting endocytosis of ox-LDL. In accordance with the above result, macrophages treated with YAM33 showed considerably less lipid accumulation and low degrees of foam cell formation, in the presence of 50 μg/mL ox-LDL, which was also dose-dependent (Fig. 3B). In contrast, free AM33 and blank YCs demonstrated less effectiveness compared to the same dose of YAM33 (Supporting Information Fig. S12).

Further, we evaluated the effects of AM33 delivered *via* YCs on the transfection and expression of target genes and proteins of miR33. Pretreatment of macrophages with YAM33 dramatically enhanced the expression of ABCA1 and ABCG1 at both the mRNA and protein levels, with the most potent activity achieved by YAM33 at 1 nmol/L (Fig. 3C and D). Consistently, remarkably higher expressions of ABCA1 and ABCG1 were also detected by flow cytometry and immunofluorescence analyses (Fig. 3E and F). Correspondingly, YAM33 effectively decreased the expression of typical proinflammatory cytokines, including IL-6, IL-1β, and TNF-α in LPS-treated macrophages (Supporting Information Fig. S13). These findings are in line with the reversed cholesterol transport and inhibited foam cell formation after treatment with YAM33.

Collectively, these data revealed that YAM33 can effectively attenuate the formation of foam cells, by increasing the expressions of ABCA1 and ABCG1 and promoting cholesterol efflux. Therefore, YAM33 may serve as a promising therapy for atherosclerosis.

3.3. *Atherosclerotic plaque-targeting capability of orally delivered YAM33 and its transport mechanisms*

According to the previous finding, YCs can be effectively internalized by macrophages that are closely associated with the pathogenesis of atherosclerosis[54,55], therefore we speculate that YCs may also transport AM33 to the chronic inflammatory sites by oral administration. To validate the plaque-targeting capacity of YAM33, atherosclerosis was established in $ApoE^{-/-}$ mice subjected to a western diet for 3 months. At 12 h post oral delivery of Cy3-YAM33, *ex vivo* imaging showed significant fluorescent signals in the isolated aortas, while no obvious fluorescence was observed in the aortas of C57BL/6 mice subject to similar treatments. The fluorescence intensity of the aortic tissues from $ApoE^{-/-}$ mice was 2.5-fold higher than that of normal aortas from C57BL/6 mice (Fig. 4A). Moreover, compared with Cy3-labeled PAM33 (*i.e.*, nanoparticles formed by AM33 and PEI), Cy3-YAM33 exhibited significantly higher fluorescent signals in the aorta (Fig. 4B). In line with this result, Cy3-YAM33-treated mice displayed higher fluorescence distribution in the intestine, liver,

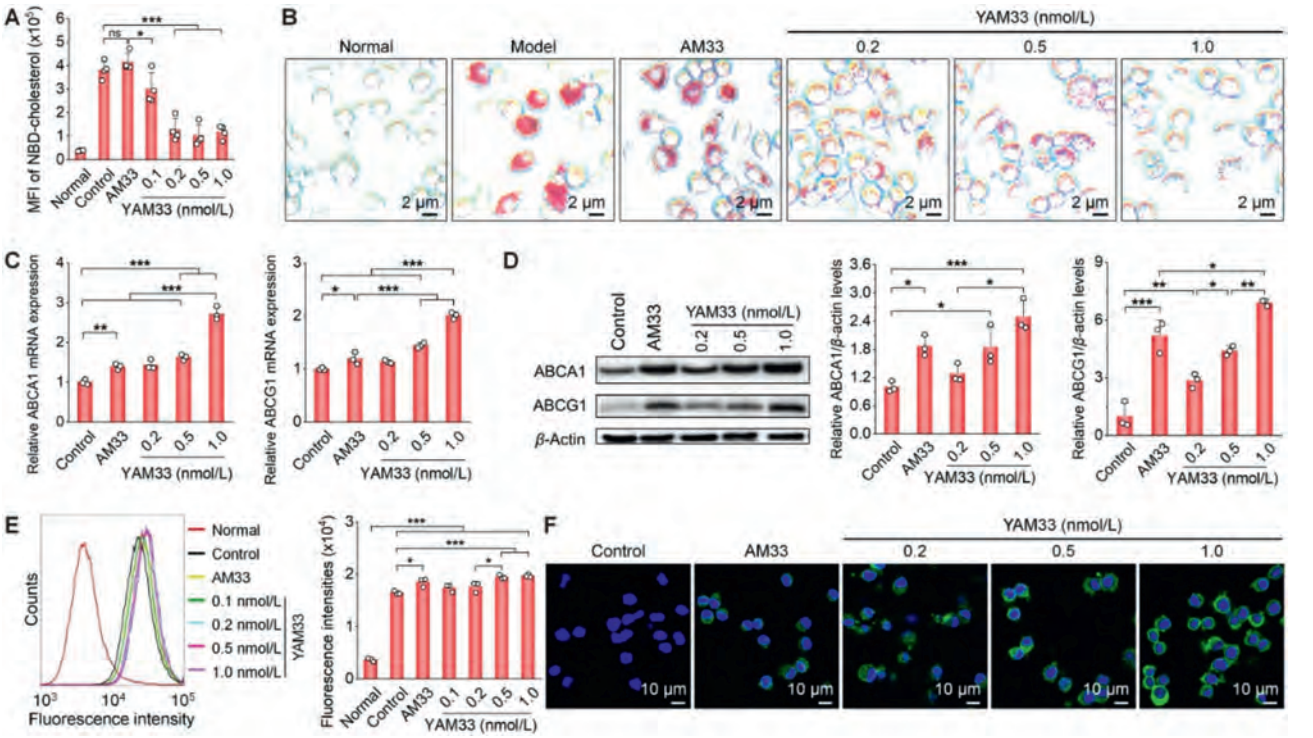

Figure 3 *In vitro* promotion of cholesterol efflux and inhibition of foam cell formation by YAM33 *via* regulating miR-33 target genes/proteins. (A) Cholesterol efflux from macrophages treated with different formulations. The dose of free AM33 was 0.2 nmol/L. MFI, mean fluorescence intensity. (B) Optical microscopy images showing ox-LDL-induced foam cell formation in macrophages after treatment with different doses of YAM33 or AM33 at 0.2 nmol/L. (C) Quantification of mRNA levels of *Abca1* (left) and *Abcg1* (right) in macrophages by real-time PCR after different treatments. (D) Western blot analysis of protein levels of ABCA1 and ABCG1 in macrophages at 8 h after indicated treatments. (E) Flow cytometric quantification of relative protein levels of ABCA1 in macrophages pretreated with different formulations for 4 h. (F) Fluorescence microscopy images showing the ABCG1 expression in macrophages treated with different formulations for 4 h. Data in (A, C−E) are presented as mean ± SD (n = 3−4). *$P < 0.05$, **$P < 0.01$, ***$P < 0.001$; ns, no significance.

and kidney (Supporting Information Fig. S14). We also examined the distribution profile of Cy3-YAM33 in different lymphatic tissues that are intimately related to the intestinal absorption of microparticles[56]. It was found that Cy3-YAM33 displayed a notably higher accumulation in the PP and MLN, in comparison to PAM33. Nevertheless, no significant differences were observed in the ILN, when Cy3-YAM33 was compared with Cy3-PAM33 (Fig. 4C).

Subsequently, mechanisms underlying the transportation and translocation of YAM33 were further investigated. At 3 h after oral administration, significant fluorescent signals were observed in the intestinal tissue of *ApoE*$^{-/-}$ mice treated with Cy3-YAM33 (Fig. 4D). Additionally, the fluorescence signal of Cy3-YAM33 in the PP, MLN, and aorta were also detected at 3 h. At 12 h, a more significant distribution of Cy3-YAM33 in the PP and whole aorta was observed (Fig. 4D and E). Immunofluorescence analysis confirmed the presence of Cy3-YAM33 in CD68^{+} macrophages isolated from the PP or aorta of *ApoE*$^{-/-}$ mice (Fig. 4F). Notably, relatively weak fluorescence was detected in the major organs, including the kidney, spleen, lung, and heart, at the examined time points (Supporting Information Fig. S15). Further, it was found that YAM33 and blank YCs showed comparable fluorescent signals in the isolated aortas and lymphatic tissues (including the PP, MLN, and ILN) of *ApoE*$^{-/-}$ mice, while no obvious fluorescence was observed in these tissues of the free AM33 group (Supporting Information Fig. S16). Additionally, the fluorescent intensities of Cy3-YAM33 in the aortas and lymphatic tissues were significantly decreased after mice were pretreated with CXI, a well-known lymphatic transport inhibitor. Consequently, both lymphatic transport and macrophage-mediated translocation are essential for plaque-targeting of orally delivered YAM33.

In a separate study, we observed that pretreatment with laminarin (a soluble β-1,3-glucan that can be recognized by Dectin-1) *via* oral delivery significantly inhibited Cy3-YAM33 accumulation in the PP (Supporting Information Fig. S17). This was confirmed by fluorescence observation of the PP section (Supporting Information Fig. S18). Furthermore, immunofluorescence analysis revealed considerable localization of Cy3-YAM33 in glycoprotein 2 (GP2)-positive M cells (Supporting Information Fig. S18). These results implied that orally delivered YAM33 was mainly translocated by M cells in intestinal PPs *via* the Dectin-1 receptor.

Also, we examined the integrity and bioactivity of YAM33 after translocation across the intestinal epithelial barrier. Direct observation by CLSM revealed intact spherical particles with diameters of 2−3 μm in the intestinal epithelial cells and M cells in the PP at 4 h after oral administration of Cy3-YAM33 (Supporting Information Fig. S19). This indicates that YAM33 remains intact before and after transport *via* M cells in the PP. In addition, the bioactivity of YAM33 after crossing a monolayer of Caco-2 epithelial cells was evaluated. The results showed that the YAM33-containing medium collected from the basolateral

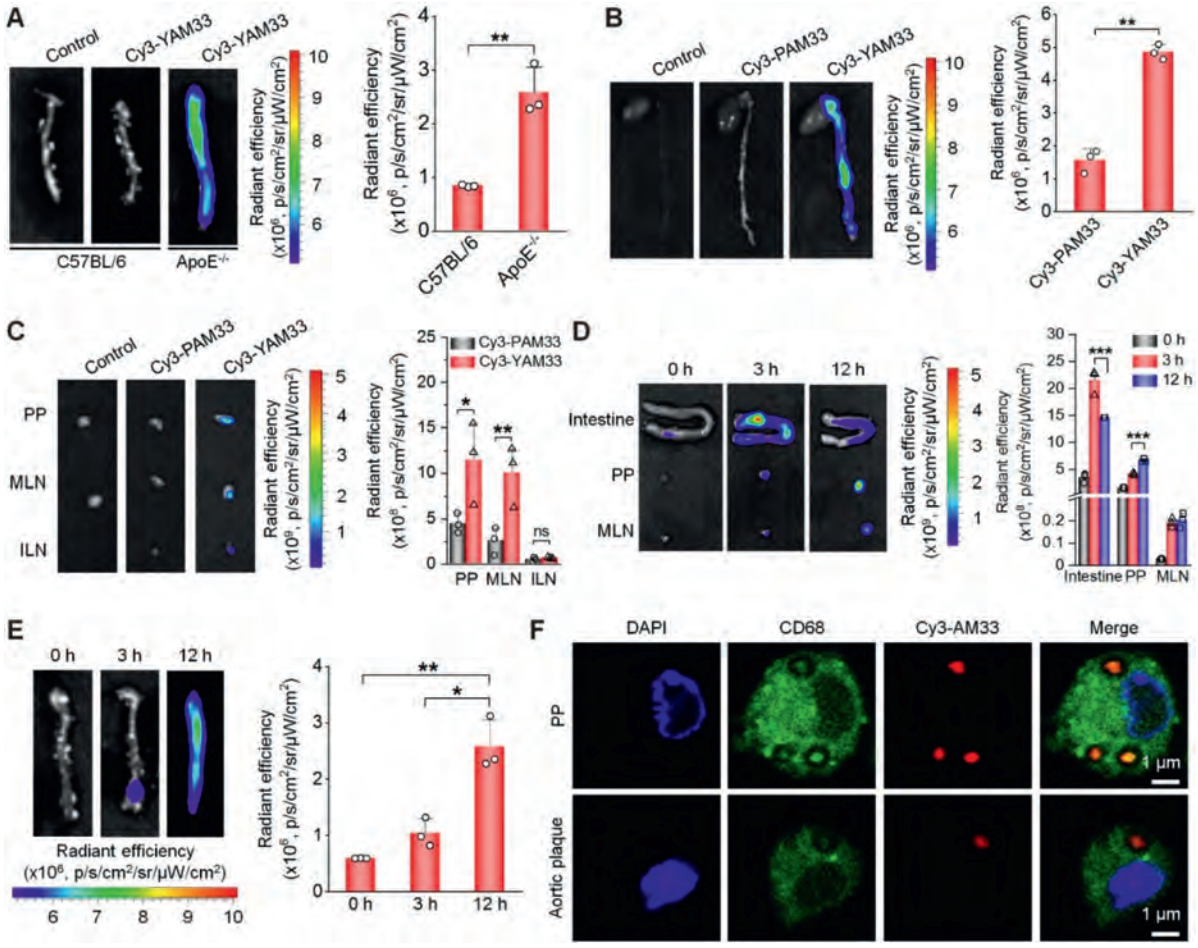

Figure 4 *In vivo* intestinal transportation and targeting of atherosclerotic plaques by orally delivered AM33 packaged in YCs. (A) *Ex vivo* images (left) and quantitative results (right) showing accumulated Cy3-YAM33 in the aortas. *ApoE*$^{-/-}$ mice fed with a western diet for 3 months or C57BL/6 mice were orally administrated with Cy3-YAM33. At 12 h after administration, mice were euthanized and aortas were isolated for *ex vivo* imaging. C57BL/6 mice in the control group were treated with the same dose of YAM33. (B) Representative *ex vivo* images (left) and quantitative analysis (right) illustrating the distribution of Cy3-PAM33 or Cy3-YAM33 in aortas with established plaques in *ApoE*$^{-/-}$ mice. (C) *Ex vivo* images (left) and quantification (right) showing transportation of Cy3-PAM33 or Cy3-YAM33 in the PP, MLN, and ILN. *ApoE*$^{-/-}$ mice fed a high-fat diet for 3 months were orally administrated with Cy3-PAM33 or Cy3-YAM33. At 12 h after administration, mice were euthanized, and PP, MLN, ILN, and aortas were isolated for *ex vivo* imaging. (D, E) *Ex vivo* images (left) and quantitative data (right) illustrating the accumulation of Cy3 fluorescent signals in the intestine, PP, MLN, and aortas. *ApoE*$^{-/-}$ mice fed a high-fat diet for 3 months were orally administrated with Cy3-YAM33. At 0, 3, or 12 h after administration, mice were euthanized. Then the intestine, PP, MLN, and aortas were isolated for *ex vivo* imaging. (F) Co-localization of Cy3-AM33 (red) and the macrophage marker CD68 (green) in cryosections of PP and aortic plaques. Data in (A−E) are presented as mean ± SD ($n = 3$). *$P < 0.05$, **$P < 0.01$, ***$P < 0.001$.

side of a Transwell plate significantly inhibited the ox-LDL-induced foam cell formation in macrophages (Supporting Information Fig. S20), indirectly demonstrating that YAM33 maintained its anti-atherosclerotic activity after translocation through a simulated intestinal barrier. Moreover, the effective transport across the epithelial cell barrier suggests that intestinal absorption of YAM33 in the PP may also be mediated by epithelial cells.

Taken together, these results substantiate that the intestinal absorption of orally delivered YAM33 is mainly mediated by M cells and epithelial cells in the PP, followed by internalization and transport by macrophages in the lymphatic system. This efficient translocation process allows YCs to notably enhance the intestinal absorption of AM33, thus improving the targeting efficiency of orally delivered AM33 to atherosclerotic lesions. Of note, the loading of AM33 does not affect the transport and tissue distribution profiles of native YCs.

3.4. *In vivo efficacy of orally delivered YAM33 in ApoE*$^{-/-}$ *mice*

Based on the above promising results, the *in vivo* therapeutic effects of YAM33 were examined. Atherosclerosis in *ApoE*$^{-/-}$ mice was established by feeding a high-fat diet for 3 months. At Week 5, *ApoE*$^{-/-}$ mice were randomly divided into 5 groups and treated with different formulations every three days (Fig. 5A). Of note, free AM33 was administered *via* subcutaneous injection, while oral delivery was also conducted for AM33/PEI nanoparticles (*i.e.*, PAM33). After 2 months, mice were euthanized and aortic tissues were excised for therapeutic evaluations. Analysis of ORO-stained whole aortas revealed remarkable atherosclerotic lesions

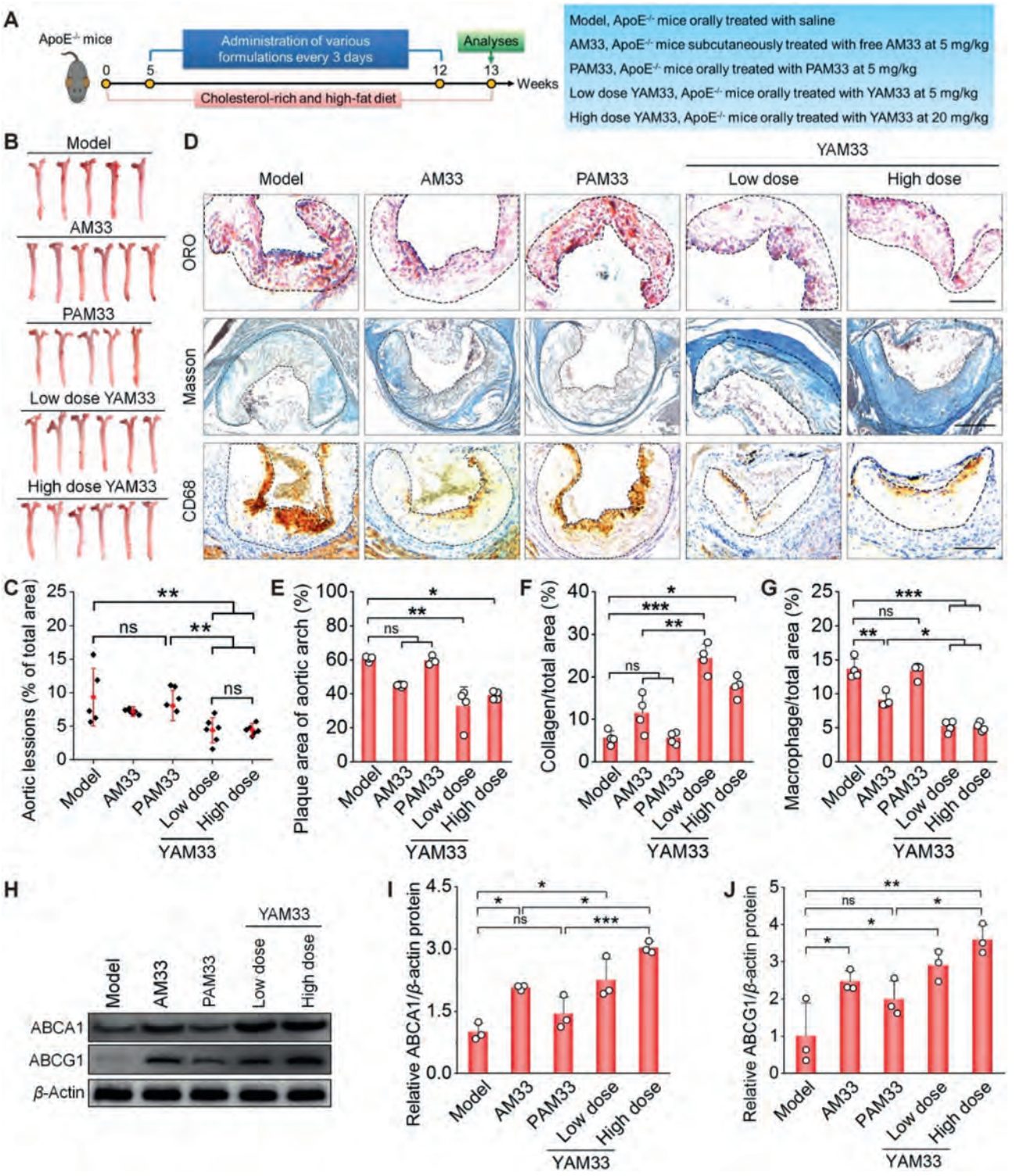

Figure 5 *In vivo* therapeutic effects of YAM33 in *ApoE*$^{-/-}$ mice with diet-induced atherosclerosis. (A) Schematic illustration of the treatment protocols. (B) Representative photographs of ORO-stained *en face* aortas from mice treated with different formulations. (C) Quantitative analysis of the lesion area in aortas. (D) Representative images of aortic root sections from *ApoE*$^{-/-}$ mice after various treatments and stained with ORO, Masson's trichrome, or anti-CD68 antibody. Scale bars, 200 μm. (E–G) Quantitative analysis of the relative areas of plaques (E), collagen (F), and macrophages (G) in sections of the aortic root. (H–J) Typical Western blot bands (H) and quantitative analysis of relative protein levels of ABCA1 (I) and ABCG1 (J) in aortas. *ApoE*$^{-/-}$ mice were fed a western diet for 3 months. After the first month, all mice received various treatments every 3 days for additional 2 months. Mice in the saline group were orally treated with saline, while other groups were separately administered with AM33 at 5 mg/kg (subcutaneous injection) as well as orally treated with PAM33 at 5 mg/kg of AM33, YAM33 at 5 mg/kg of AM33 (low dose), or YAM33 at 20 mg/kg of AM33 (high dose). Data in (C, E–G, I, J) are presented as mean ± SD (n = 3–6). *P < 0.05, **P < 0.01, ***P < 0.001; ns, no significance.

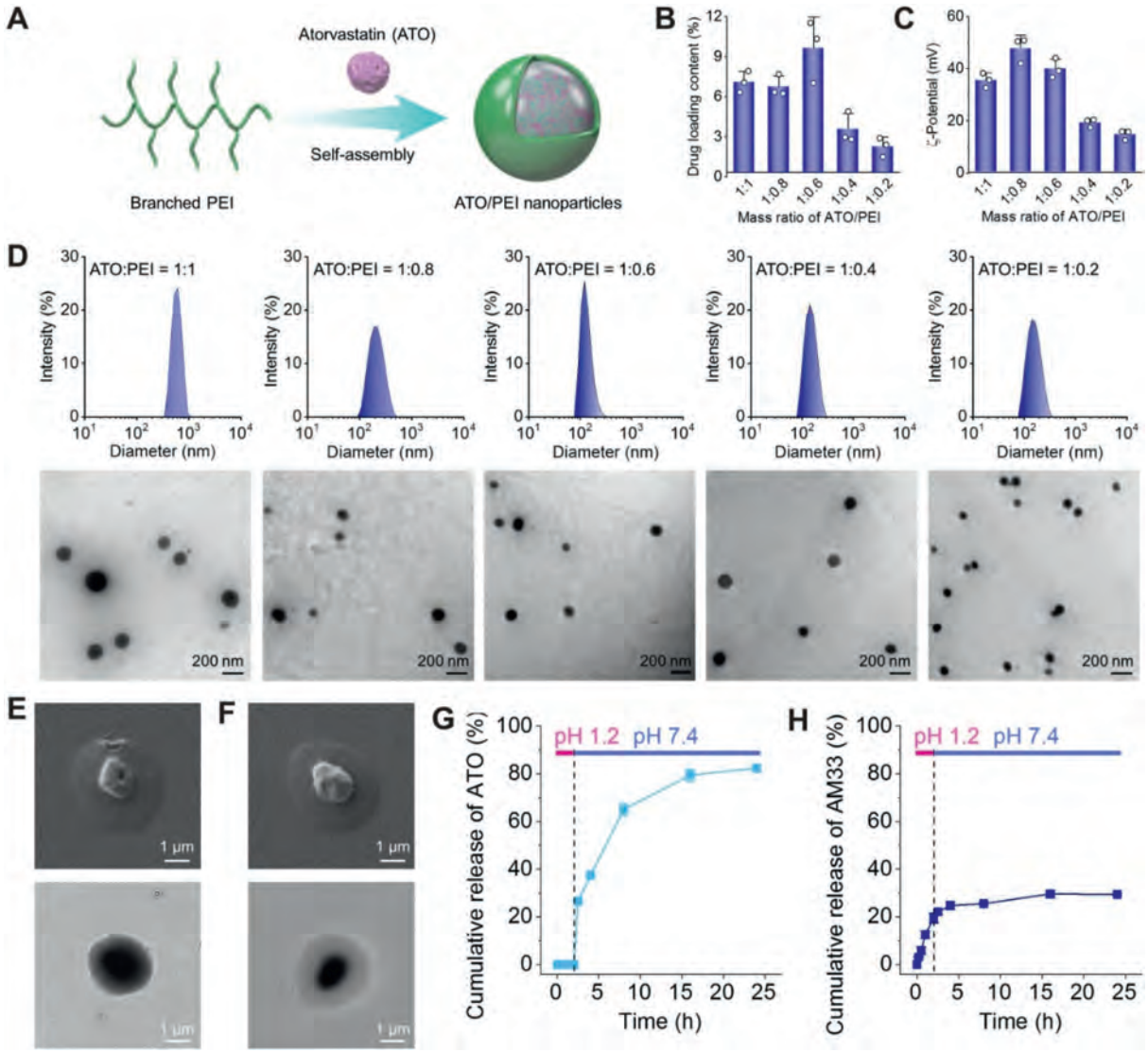

Figure 6 Fabrication and characterization of YCs loaded with ATO and AM33. (A) A sketch showing the self-assembly of ATO/PEI nanoparticles. (B) Loading contents of ATO in ATO/PEI nanoparticles obtained at various weight ratios of ATO to PEI. (C) ζ-Potential values of ATO/PEI nanoparticles assembled at different ATO/PEI weight ratios. (D) Size distribution profiles (upper panels) and TEM images (lower panels) of ATO/PEI nanoparticles formulated at various ATO/PEI weight ratios. (E,F) TEM (upper) and SEM (lower) images of the finally screened YC loaded with ATO/PEI nanoparticles alone (*i.e.*, YATO) (E) and YC loaded with ATO/PEI nanoparticles and AM33 (*i.e.*, YAA) (F). (G,H) *In vitro* release profiles of ATO (G) and AM33 (H) from YAA in aqueous solutions simulating gastrointestinal conditions. Data in (B,C,G,H) are presented as mean ± SD ($n = 3$).

in *ApoE*$^{-/-}$ mice treated with saline (Fig. 5B and C). Comparable ORO-stained areas were also measured in the aortas of mice subjected to PAM33 treatment at 5 mg/kg of AM33 by oral gavage. Naked AM33 at 5 mg/kg delivered *via* subcutaneous injection only slightly decreased the plaque area, affording limited therapeutic efficacy. By contrast, we found significantly smaller lesion areas in aortas isolated from mice orally treated with YAM33 at the low (5 mg/kg) and high (20 mg/kg) doses of AM33. Similar results were observed in ORO-stained cryosections of aortic roots isolated from different groups (Fig. 5D and E). In a separate study, the possible *in vivo* efficacy of blank YCs was investigated in *ApoE*$^{-/-}$ mice. As compared to the model group, blank YCs only slightly reduced the lesion area (Supporting Information Fig. S21), showing no statistical significance.

Histological examination after Masson's trichrome-staining of aortic sections indicated notably high contents of collagen around plaques in two YAM33 groups, as compared to those of other groups (Fig. 5D and F). Moreover, immunohistochemistry analysis revealed the smallest CD68-positive areas for the YAM33-treated groups, implying the considerably attenuated accumulation of macrophages (Fig. 5D and G). According to previous findings, macrophages in the plaques may facilitate the formation of vulnerable lesions, while thick fibrous caps, primarily consisting of collagen, contribute to plaque stability[57]. Correspondingly, YAM33 also effectively reduced the expression of typical proinflammatory cytokines, including TNF-α and IL-1β (Supporting Information Fig. S22). Accordingly, oral treatment with YAM33 can improve the stability of plaques.

Subsequently, we determined the *in vivo* effects of orally delivered YAM33 on the expressions of target proteins of miR-33. In this aspect, significantly higher protein levels of ABCA1 and ABCG1 were detected in the aorta of mice treated with YAM33 (Fig. 5H−J). Whereas free AM33 could also increase ABCA1 and ABCG1 expressions, their levels were considerably lower than those of the YAM33 groups. Orally delivered PAM33 showed no significant effects on both ABCA1 and ABCG1 levels, compared to the model group. These data are consistent with the above findings on the plaque area and compositions.

Taken together, our results demonstrated that oral treatment with YAM33 can effectively delay the progression of atherosclerosis by increasing the expression of ABCA1 and ABCG1, lowering the infiltration of macrophages in plaques, and inhibiting the formation of vulnerable plaques. This potent efficacy of YAM33 should be due to the enhanced stability and increased absorption of AM33 in the gastrointestinal tract as well as promoted plaque targeting *via* the hitchhiking effect of macrophages.

3.5. Engineering of YCs simultaneously loaded with AM33 and atorvastatin

On the basis of promising therapeutic effects achieved by orally delivered YAM33, we hypothesize that combination therapy of atherosclerosis can be easily realized *via* the YC-based oral targeting strategy. As a proof of concept, AM33 and atorvastatin (ATO) were co-encapsulated in YCs, in view of the fact that ATO can lower lipid levels, stabilize atherosclerotic plaques, and promote atherosclerosis regression. According to our previous studies, hydrophobic therapeutics bearing carboxyl groups can interact with amino-containing polymer PEI *via* electrostatic forces and hydrogen bonding, thereby self-assembling into positively charged nanoparticles[58,59]. Herein, ATO/PEI nanoparticles were formulated by this strategy (Fig. 6A). The impact of the ATO/PEI weight ratio on the formation of nanoparticles and drug loading was first examined. Among all tested ATO/PEI weight ratios, nanoparticles formed at 1:0.6 exhibited the highest drug loading content (Fig. 6B). Positive ζ-potential values were detected for nanoparticles assembled at various weight ratios of ATO/PEI (Fig. 6C). In addition, all nanoparticles showed monodispersed size distribution profiles and well-defined spherical structures (Fig. 6D). The average diameter of ATO/PEI nanoparticles was increased from 144 to 554 nm as the ATO/PEI weight ratio varied from 1:0.2 to 1:1. Consequently, ATO/PEI nanoparticles (with the mean diameter of 189.4 nm and ζ-potential of 40.0 mV) assembled at the ATO/PEI weight ratio of 1:0.6 was used to prepare ATO-loaded YCs (defined as YATO) by simply incubating with YCs.

Characterization by SEM and TEM revealed a densely packaged core for the obtained YATO (Fig. 6E), with a ζ-potential of 31 mV. Then YCs co-packaged with ATO and AM33 were prepared by incubation of YATO with AM33, taking advantage of electrostatic interactions between AM33 and positively charged ATO/PEI nanoparticles deposited in YCs. YCs containing both ATO and AM33, defined as YAA, also displayed a densely loaded core (Fig. 6F), comparable to that of YATO. The average size of YAA was 2.3 μm, and its ζ-potential was 30.1 mV. The entrapment efficiency of ATO and AM33 in YAA was found to be 52.1 $\pm$ 3.9% and 83.3 $\pm$ 1.4%, while the corresponding drug loading content was 4.4 $\pm$ 0.7% and 2.8 $\pm$ 0.3%, respectively. *In vitro* tests indicated nearly no ATO release from YAA in a simulated gastric fluid, while it was rapidly released in a simulated intestinal fluid (Fig. 6G). For AM33, its release profile from YAA was similar to that of YAM33 (Fig. 6H). Further, HPLC analysis indicated that ATO encapsulated in YCs could be clearly detected after incubation with simulated gastric or intestinal fluids for 4 h, while free ATO was unstable in the examined solutions, especially in the gastric fluid (Supporting Information Fig. S23). Of note, carboxylic acid-containing ATO can be easily transformed into the lactone form in the presence of gastric acid[60]. Together, the nucleic acid drug AM33 and clinically used small-molecule drug ATO can be efficiently loaded into YCs by a facile self-assembly and deposition strategy. The newly engineered YAA is able to protect the encapsulated nucleic acid and small-molecular drug from degradation, thus achieving synergistic anti-atherosclerotic efficacy.

3.6. Therapeutic effects of orally delivered YAA in ApoE$^{-/-}$ mice

We then interrogated the *in vivo* efficacies of YAA. In this case, more severe atherosclerotic plaques were induced in *ApoE*$^{-/-}$ mice by a Western diet for 4 months (Fig. 7A). After 4 weeks, randomly assigned mice were orally treated with different formulations every 3 days. At week 17, mice were euthanized for therapeutic evaluations. Direct observation and quantitative analysis of ORO-stained whole aortas suggested that oral administration of YATO, YAM33, and YAA reduced the atherosclerotic lesion areas, to much more significant degrees than free ATO (Fig. 7B and C). Among various formulations, YAA afforded the best efficacy. Inspection of ORO-stained aortic root sections showed similar results (Fig. 7D and E). Also, treatment with different formulations effectively increased the collagen content and decreased the macrophage infiltration in aortic tissues, as implicated by histological examination (Fig. 7D, F, and G). Again, YAA was more efficacious than YATO and YAM33, mainly due to the synergistic effect of AM33 and ATO.

In addition, examination on H&E or ORO-stained liver sections indicated that intracellular lipid droplets in the liver were also most effectively reduced after YAA treatment (Fig. 8A). Furthermore, whereas interventions with different formulations could reduce the levels of total cholesterol and triglyceride as well as increase the HDL levels in the blood serums (Fig. 8B−D), the most significant effects were achieved by orally delivered YAA. Collectively, these results demonstrated that co-delivery of AM33 and ATO *via* YCs further potentiates the *in vivo* anti-atherosclerotic efficacy of YAM33 by synergistically lowering the contents of lipids and increasing the HDL level. These findings also suggested that YCs can be employed as an effective biomimetic platform for co-delivering different types of anti-atherosclerotic agents *via* the oral route.

3.7. Safety profiles of various YCs

Finally, safety studies were conducted for different YC-based formulations. *In vitro* experiments indicated that YAM33 and YAA exhibited almost no cytotoxicity in both RAW264.7 macrophages and BMDMs (Supporting Information Figs. S24 and S25), at the examined doses. The possible side effects after long-term treatment with various YCs were also examined *in vivo*. During the course of treatment, the body weight of all the treated mice gradually increased, with no significant differences observed between the groups (Supporting Information Fig. S26). Analysis on the organ index of major organs including the liver, spleen,

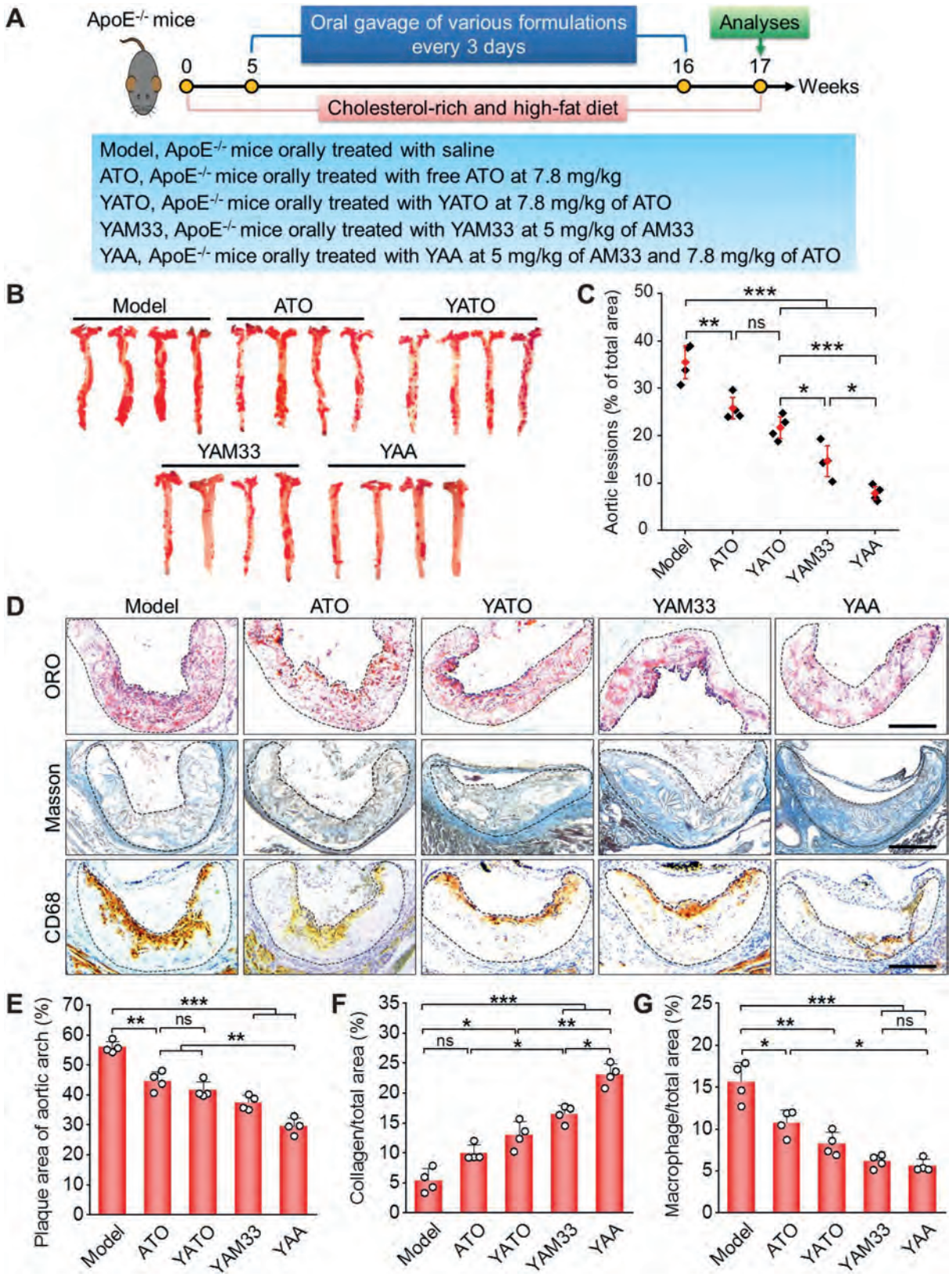

Figure 7 Therapeutic effects of orally delivered YAA in *ApoE*$^{-/-}$ mice. (A) Schematic illustration of the treatment protocols. (B) Representative photographs of *en face* ORO-stained aortas from mice after treatment with different formulations. (C) Quantitative results of the lesion area in aortas. (D) Representative images of aortic root sections stained with ORO, Masson's trichrome, or anti-CD68 antibody. Scale bars, 200 μm. (E–G) Quantitative analysis of the relative areas of plaques (E), collagen (F), and macrophages (G) in sections of the aortic root. *ApoE*$^{-/-}$ mice were fed a western diet for 4 months. After the first month, all mice were orally administered various formulations every 3 days for

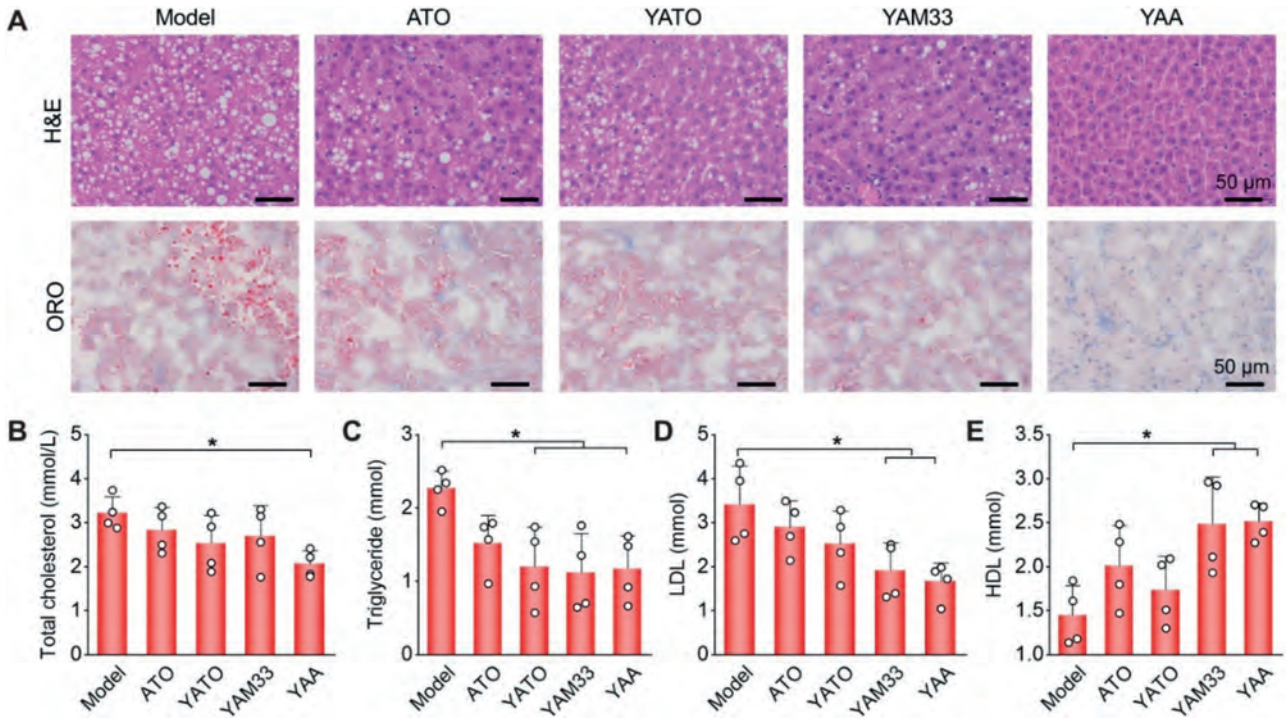

Figure 8 *In vivo* regulation of lipids in $ApoE^{-/-}$ mice after treatment with different formulations. (A) Representative photographs of liver sections stained with H&E or ORO. Scale bars, 50 μm. (B−E) The serum levels of total cholesterol (B), triglyceride (C), and HDL (D). Data in (B−D) are presented as mean ± SD ($n = 4$). *$P < 0.05$.

lung, and kidney also demonstrated no significant differences among different groups (Supporting Information Fig. S27). Measurement of typical hematological parameters (including red blood cells, white blood cells, hemoglobin, and platelets) revealed no abnormal deviations in different groups. Moreover, the levels of typical biochemical markers relevant to hepatic and kidney functions did not show abnormal elevations (Supporting Information Fig. S28). Further examination on H&E-stained sections of major organs and gastrointestinal tissues indicated no obvious damage in all YC formulation-treated mice (Supporting Information Figs. S29 and S30). These preliminary results demonstrated that YCs containing ATO, AM33, or ATO/AM33 display good safety performance for oral gavage at the examined dose.

4. Conclusions

In summary, we successfully engineered orally deliverable biomimetic nucleic acid therapies by efficiently loading an antisense oligonucleotide AM33 or co-loading AM33 and a small-molecular drug into yeast-derived microcapsules (*i.e.*, YCs) for targeted treatment of atherosclerosis. The constructed AM33-loaded YCs (YAM33) can be rapidly internalized in macrophages and intracellularly transported through the endolysosomal pathway, thus effectively promoting cholesterol efflux and inhibiting foam cell formation by up-regulating gene/protein expressions of ABCA1 and ABCG1 in macrophages. Orally delivered YAM33 effectively accumulated in atherosclerotic plaques in the aortas of $ApoE^{-/-}$ mice, primarily by trans-epithelial absorption *via* M cells in Peyer's patches and subsequent translocation *via* macrophages through the lymphatic system. In $ApoE^{-/-}$ mice with established atherosclerosis, oral treatment with YAM33 significantly reduced the plaque area in the aortas and improved plaque stability. By simultaneously packaging AM33 and ATO (a clinically frequently used lipid-lowering drug) into YCs, an oral targeting combination therapy YAA was developed, which afforded significantly potentiated *in vivo* anti-atherosclerotic efficacy by synergistic effects of co-payloads. Moreover, preliminary studies showed good safety profiles of YAM33 and YAA after long-term oral delivery. To the best of our knowledge, YAM33/YAA represents the first orally deliverable anti-atherosclerotic nucleic acid therapy examined thus far. Moreover, compared with other delivery vectors investigated for gene therapy of atherosclerosis, such as lentiviruses[44], cationic lipid or polymer NPs[61-63], cationic lipid/polymer hybrid NPs[64,65], and bilayered NPs[66], our YCs-based delivery platform owns multiple advantages like easy preparation, low cost, high loading efficiency for nucleic acids, and good biocompatibility. In addition to AM33, this yeast-based platform can be employed for oral delivery of other nucleic acids (such as siRNA, miRNA, and mRNA), either alone or in combination with existing drugs, for precision therapy of atherosclerotic diseases.

an additional 3 months. The model group was treated with saline alone, while other groups were separately administered ATO at 7.8 mg/kg, YATO at 7.8 mg/kg of ATO, YAM33 at 5 mg/kg of AM33, or YAA at 5 mg/kg AM33 and 7.8 mg/kg ATO. Data in (C, E−G) are presented as mean ± SD ($n = 4$). *$P < 0.05$, **$P < 0.01$, ***$P < 0.001$; ns, no significance.

Acknowledgments

This work was supported by the National Natural Science Foundation of China, China (Nos. 32301198 and 32271451), China Postdoctoral Science Foundation, China (No. 2022M713832), Natural Science Foundation of Chongqing, China (No. CSTB2022NSCQ-MSX0939), New Chongqing Youth Innovative Talent Program (No. CSTB2024NSCQ-QCXMX0005), and Graduate Supervisor Team Program of Chongqing in 2022.

Author contributions

Chenwen Li: Writing − review & editing, Funding acquisition, Writing − original draft, Project administration, Methodology. Yidan Chen: Writing − original draft, Methodology, Investigation. Yuan Li: Writing − original draft, Methodology, Investigation. Huan Liu: Writing − original draft, Methodology, Investigation. Shengqian Yang: Writing − original draft, Investigation. Yongyao Lin: Methodology, Investigation. Yuantong Qi: Investigation. Songling Han: Writing − original draft, Investigation. Yin Dou: Project administration, Methodology. Gaoxing Luo: Supervision, Project administration, Writing − review & editing, Funding acquisition. Yingxue Hao: Supervision, Project administration, Writing − review & editing, Funding acquisition. Jianxiang Zhang: Writing − review & editing, Supervision, Project administration, Funding acquisition, Conceptualization, Writing − original draft.

Conflicts of interest

The authors have no conflicts of interest to declare.

Appendix A. Supporting information

Supporting information to this article can be found online at https://doi.org/10.1016/j.apsb.2025.07.039.

References

1. Libby P. The changing landscape of atherosclerosis. *Nature* 2021;**592**:524−33.
2. Bäck M, Yurdagul A, Tabas I, Öörni K, Kovanen PT. Inflammation and its resolution in atherosclerosis: mediators and therapeutic opportunities. *Nat Rev Cardiol* 2019;**16**:389−406.
3. Preiss D, Tobert Jonathan A, Hovingh GK, Reith C. Lipid-modifying agents, from statins to PCSK9 inhibitors. *J Am Coll Cardiol* 2020;**75**:1945−55.
4. Dadu RT, Ballantyne CM. Lipid lowering with PCSK9 inhibitors. *Nat Rev Cardiol* 2014;**11**:563−75.
5. Cholesterol Treatment Trialists Collaborators, Kearney PM, Blackwell L, Collins R, Keech A, Simes J, et al. Efficacy of cholesterol-lowering therapy in 18686 people with diabetes in 14 randomised trials of statins: a meta-analysis. *Lancet* 2008;**371**:117−25.
6. Baigent C, Keech A, Kearney PM, Blackwell L, Buck G, Pollicino C, et al. Efficacy and safety of cholesterol-lowering treatment: prospective meta-analysis of data from 90,056 participants in 14 randomised trials of statins. *Lancet* 2005;**366**:1267−78.
7. Andrade RJ, Chalasani N, Björnsson ES, Suzuki A, Kullak-Ublick GA, Watkins PB, et al. Drug-induced liver injury. *Nat Rev Dis Primers* 2019;**5**:58.
8. Kazi DS, Moran AE, Coxson PG, Penko J, Ollendorf DA, Pearson SD, et al. Cost-effectiveness of PCSK9 inhibitor therapy in patients with heterozygous familial hypercholesterolemia or atherosclerotic cardiovascular disease. *JAMA* 2016;**316**:743−53.
9. Tokgözoğlu L, Libby P. The dawn of a new era of targeted lipid-lowering therapies. *Eur Heart J* 2022;**43**:3198−208.
10. Qu S, Liu RF, Zhang NS, Xu YX, Yue XL, Dai ZF. Non-viral nucleic acid therapeutics: revolutionizing the landscape of atherosclerotic treatment. *Nano Today* 2022;**45**:101514.
11. Li XX, Qi HZ, Cui WG, Wang ZB, Fu XX, Li TX, et al. Recent advances in targeted delivery of non-coding RNA-based therapeutics for atherosclerosis. *Mol Ther* 2022;**30**:3118−32.
12. Hetherington I, Totary-Jain H. Anti-atherosclerotic therapies: milestones, challenges, and emerging innovations. *Mol Ther* 2022;**30**:3106−17.
13. Feinberg MW, Moore KJ. MicroRNA regulation of atherosclerosis. *Circ Res* 2016;**118**:703−20.
14. van Rooij E, Olson EN. MicroRNA therapeutics for cardiovascular disease: opportunities and obstacles. *Nat Rev Drug Discov* 2012;**11**:860−72.
15. Gouni-Berthold I, Alexander VJ, Yang Q, Hurh E, Steinhagen-Thiessen E, Moriarty PM, et al. Efficacy and safety of volanesorsen in patients with multifactorial chylomicronaemia (COMPASS): a multicentre, double-blind, randomised, placebo-controlled, phase 3 trial. *Lancet Diabetes Endocrinol* 2021;**9**:264−75.
16. Gaudet D, Karwatowska-Prokopczuk E, Baum SJ, Hurh E, Kingsbury J, Bartlett VJ, et al. Vupanorsen, an *N*-acetyl galactosamine-conjugated antisense drug to ANGPTL3 mRNA, lowers triglycerides and atherogenic lipoproteins in patients with diabetes, hepatic steatosis, and hypertriglyceridaemia. *Eur Heart J* 2020;**41**:3936−45.
17. Paik J, Duggan S. Volanesorsen: first global approval. *Drugs* 2019;**79**:1349−54.
18. Ray KK, Wright RS, Kallend D, Koenig W, Leiter LA, Raal FJ, et al. Two phase 3 trials of Inclisiran in patients with elevated LDL cholesterol. *N Engl J Med* 2020;**382**:1507−19.
19. Roberts TC, Langer R, Wood MJA. Advances in oligonucleotide drug delivery. *Nat Rev Drug Discov* 2020;**19**:673−94.
20. Cui K, Gao XL, Wang BB, Wu H, Arulsamy K, Dong YZ, et al. Epsin nanotherapy regulates cholesterol transport to fortify atheroma regression. *Circ Res* 2023;**132**:e22−42.
21. Zhang XB, Rotllan N, Canfrán-Duque A, Sun J, Toczek J, Moshnikova A, et al. Targeted suppression of miRNA-33 using pHLIP improves atherosclerosis regression. *Circ Res* 2022;**131**:77−90.
22. Huang XG, Liu C, Kong N, Xiao YF, Yurdagul A, Tabas I, et al. Synthesis of siRNA nanoparticles to silence plaque-destabilizing gene in atherosclerotic lesional macrophages. *Nat Protoc* 2022;**17**:748−80.
23. Chen W, Schilperoort M, Cao YH, Shi JJ, Tabas I, Tao W. Macrophage-targeted nanomedicine for the diagnosis and treatment of atherosclerosis. *Nat Rev Cardiol* 2022;**19**:228−49.
24. Tao W, Yurdagul A, Kong N, Li WL, Wang XB, Doran AC, et al. SiRNA nanoparticles targeting CAMKIIγ in lesional macrophages improve atherosclerotic plaque stability in mice. *Sci Transl Med* 2020;**12**:eaay1063.
25. Li CW, Dou Y, Chen YD, Qi YT, Li LL, Han SL, et al. Site-specific microRNA-33 antagonism by pH-responsive nanotherapies for treatment of atherosclerosis *via* regulating cholesterol efflux and adaptive immunity. *Adv Funct Mater* 2020;**30**:2002131.
26. Wang CL, Xu MC, Fan QZ, Li CH, Zhou XY. Therapeutic potential of exosome-based personalized delivery platform in chronic inflammatory diseases. *Asian J Pharm Sci* 2023;**18**:100772.
27. Tao Y, Lan XM, Zhang Y, Fu CX, Liu L, Cao F, et al. Biomimetic nanomedicines for precise atherosclerosis theranostics. *Acta Pharm Sin B* 2023;**13**:4442−60.
28. Tang J, Lobatto ME, Hassing L, van der Staay S, van Rijs SM, Calcagno C, et al. Inhibiting macrophage proliferation suppresses atherosclerotic plaque inflammation. *Sci Adv* 2015;**1**:e1400223.
29. Lobatto ME, Calcagno C, Millon A, Senders ML, Fay F, Robson PM, et al. Atherosclerotic plaque targeting mechanism of long-circulating nanoparticles established by multimodal imaging. *ACS Nano* 2015;**9**:1837−47.

30. Lobatto ME, Fuster V, Fayad ZA, Mulder WJM. Perspectives and opportunities for nanomedicine in the management of atherosclerosis. *Nat Rev Drug Discov* 2011;**10**:835−52.
31. Wei XL, Ying M, Dehaini D, Su YY, Kroll AV, Zhou JR, et al. Nanoparticle functionalization with platelet membrane enables multifactored biological targeting and detection of atherosclerosis. *ACS Nano* 2018;**12**:109−16.
32. Fan WF, Wei QY, Xiang JJ, Tang YS, Zhou Q, Geng Y, et al. Mucus penetrating and cell-binding polyzwitterionic micelles as potent oral nanomedicine for cancer drug delivery. *Adv Mater* 2022;**34**:2109189.
33. Lamson NG, Berger A, Fein KC, Whitehead KA. Anionic nanoparticles enable the oral delivery of proteins by enhancing intestinal permeability. *Nat Biomed Eng* 2020;**4**:84−96.
34. Pridgen EM, Alexis F, Kuo TT, Levy-Nissenbaum E, Karnik R, Blumberg RS, et al. Transepithelial transport of Fc-targeted nanoparticles by the neonatal Fc receptor for oral delivery. *Sci Transl Med* 2013;**5**:213ra167.
35. Zhou X, Zhang XJ, Han SL, Dou Y, Liu MY, Zhang L, et al. Yeast microcapsule-mediated targeted delivery of diverse nanoparticles for imaging and therapy *via* the oral route. *Nano Lett* 2017;**17**:1056−64.
36. Hu XK, Zhang JX. Yeast capsules for targeted delivery: the future of nanotherapy?. *Nanomedicine* 2017;**12**:955−7.
37. Aouadi M, Tesz GJ, Nicoloro SM, Wang M, Chouinard M, Soto E, et al. Orally delivered siRNA targeting macrophage MAP4K4 suppresses systemic inflammation. *Nature* 2009;**458**:1180−4.
38. Zhang XJ, Xu XQ, Chen YD, Dou Y, Zhou X, Li LL, et al. Bioinspired yeast microcapsules loaded with self-assembled nanotherapies for targeted treatment of cardiovascular disease. *Mater Today* 2017;**20**:301−13.
39. Zhou X, Ling KJ, Liu MY, Zhang XJ, Ding J, Dong Y, et al. Targeted delivery of cisplatin-derived nanoprecursors *via* a biomimetic yeast microcapsule for tumor therapy by the oral route. *Theranostics* 2019;**9**:6568−86.
40. Zhang L, Peng H, Zhang W, Li YK, Liu L, Leng TT. Yeast cell wall particle mediated nanotube-RNA delivery system loaded with miR365 antagomir for post-traumatic osteoarthritis therapy *via* oral route. *Theranostics* 2020;**10**:8479−93.
41. Sabu C, Raghav D, Jijith US, Mufeedha P, Naseef PP, Rathinasamy K, et al. Bioinspired oral insulin delivery system using yeast microcapsules. *Mater Sci Eng C* 2019;**103**:109753.
42. Zhang X, Zhao YY, Xu Y, Pan YM, Chen F, Kumar A, et al. *In situ* self-assembly of peptides in glucan particles for macrophage-targeted oral delivery. *J Mater Chem B* 2014;**2**:5882−90.
43. Tesz Gregory J, Aouadi M, Prot M, Nicoloro Sarah M, Boutet E, Amano Shinya U, et al. Glucan particles for selective delivery of siRNA to phagocytic cells in mice. *Biochem J* 2011;**436**:351−62.
44. Rayner KJ, Suárez Y, Dávalos A, Parathath S, Fitzgerald ML, Tamehiro N, et al. MiR-33 contributes to the regulation of cholesterol homeostasis. *Science* 2010;**328**:1570−3.
45. Horie T, Baba O, Kuwabara Y, Chujo Y, Watanabe S, Kinoshita M, et al. MicroRNA-33 deficiency reduces the progression of atherosclerotic plaque in $ApoE^{-/-}$ mice. *J Am Heart Assoc* 2012;**1**:e003376.
46. Price NL, Rotllan N, Zhang X, Canfrán-Duque A, Nottoli T, Suarez Y, et al. Specific disruption of Abca1 targeting largely mimics the effects of miR-33 knockout on macrophage cholesterol efflux and atherosclerotic plaque development. *Circ Res* 2019;**124**:874−80.
47. Ouimet M, Ediriweera H, Afonso MS, Ramkhelawon B, Singaravelu R, Liao X, et al. MicroRNA-33 regulates macrophage autophagy in atherosclerosis. *Arterioscler Thromb Vasc Biol* 2017;**37**:1058−67.
48. Rayner KJ, Esau CC, Hussain FN, McDaniel AL, Marshall SM, van Gils JM, et al. Inhibition of miR-33a/b in non-human primates raises plasma HDL and lowers VLDL triglycerides. *Nature* 2011;**478**:404−7.
49. Marquart TJ, Allen RM, Ory DS, Baldán Á. MiR-33 links SREBP-2 induction to repression of sterol transporters. *Proc Natl Acad Sci* 2010;**107**:12228−32.
50. Afonso MS, Sharma M, Schlegel M, van Solingen C, Koelwyn GJ, Shanley LC, et al. MiR-33 silencing reprograms the immune cell landscape in atherosclerotic plaques. *Circ Res* 2021;**128**:1122−38.
51. Soto ER, Ostroff GR. Characterization of multilayered nanoparticles encapsulated in yeast cell wall particles for DNA delivery. *Bioconjug Chem* 2008;**19**:840−8.
52. Boussif O, Lezoualc'h F, Zanta MA, Mergny MD, Scherman D, Demeneix B, et al. A versatile vector for gene and oligonucleotide transfer into cells in culture and *in vivo*: polyethylenimine. *Proc Natl Acad Sci U S A* 1995;**92**:7297−301.
53. Roy S, Zhu DC, Parak WJ, Feliu N. Lysosomal proton buffering of poly(ethylenimine) measured *in situ* by fluorescent pH-sensor microcapsules. *ACS Nano* 2020;**14**:8012−23.
54. Swirski FK, Nahrendorf M. Leukocyte behavior in atherosclerosis, myocardial infarction, and heart failure. *Science* 2013;**339**:161−6.
55. Moore Kathryn J, Tabas I. Macrophages in the pathogenesis of atherosclerosis. *Cell* 2011;**145**:341−55.
56. Jenkins PG, Howard KA, Blackball NW, Thomas NW, Davis SS, O'Hagan DT. Microparticulate absorption from the rat intestine. *J Control Release* 1994;**29**:339−50.
57. Silvestre-Roig C, de Winther MP, Weber C, Daemen MJ, Lutgens E, Soehnlein O. Atherosclerotic plaque destabilization: mechanisms, models, and therapeutic strategies. *Circ Res* 2014;**114**:214−26.
58. Zhou X, Che L, Wei YL, Dou Y, Chen S, He HM, et al. Facile route to versatile nanoplatforms for drug delivery by one-pot self-assembly. *Acta Biomater* 2014;**10**:2630−42.
59. Cheng J, Feng SB, Han SL, Zhang XJ, Chen YD, Zhou X, et al. Facile assembly of cost−effective and locally applicable or injectable nanohemostats for hemorrhage control. *ACS Nano* 2016;**10**:9957−73.
60. Morse BL, Alberts JJ, Posada MM, Rehmel J, Kolur A, Tham LS, et al. Physiologically-based pharmacokinetic modeling of atorvastatin incorporating delayed gastric emptying and acid-to-lactone conversion. *CPT Pharmacometrics Syst Pharmacol* 2019;**8**:664−75.
61. Nguyen MA, Wyatt H, Susser L, Geoffrion M, Rasheed A, Duchez AC, et al. Delivery of microRNAs by chitosan nanoparticles to functionally alter macrophage cholesterol efflux *in vitro* and *in vivo*. *ACS Nano* 2019;**13**:6491−505.
62. Gadde S, Rayner KJ. Nanomedicine meets microRNA: current advances in RNA-based nanotherapies for atherosclerosis. *Arterioscler Thromb Vasc Biol* 2016;**36**:e73−9.
63. Kheirolomoom A, Kim CW, Seo JW, Kumar S, Son DJ, Gagnon MKJ, et al. Multifunctional nanoparticles facilitate molecular targeting and miRNA delivery to inhibit atherosclerosis in $ApoE^{-/-}$ mice. *ACS Nano* 2015;**9**:8885−97.
64. Lu J, Zhao Y, Zhou XJ, He JH, Yang Y, Jiang CP, et al. Biofunctional polymer−lipid hybrid high-density lipoprotein-mimicking nanoparticles loading anti-miR155 for combined antiatherogenic effects on macrophages. *Biomacromolecules* 2017;**18**:2286−95.
65. Sager HB, Dutta P, Dahlman JE, Hulsmans M, Courties G, Sun Y, et al. RNAi targeting multiple cell adhesion molecules reduces immune cell recruitment and vascular inflammation after myocardial infarction. *Sci Transl Med* 2016;**8**:342ra80.
66. Zhu XW, Xie HZ, Liang XY, Li XL, Duan JW, Chen YX, et al. Bilayered nanoparticles with sequential release of *VEGF* gene and paclitaxel for restenosis inhibition in atherosclerosis. *ACS Appl Mater Interfaces* 2017;**9**:27522−32.